Pure Appl. Chem., Vol. 71, No. 6, pp. 951–978, 1999.
Printed in Great Britain.

Passivity—the key to our metals-based civilization*

Digby D. Macdonald

Pure and Applied Physical Sciences Division, SRI International, Menlo Park, CA 94025, USA

Abstract: Humankind has been able to develop a metals-based civilization primarily because the reactive metals (Fe, Ni, Cr, Al, Ti, Zr, …) exhibit extraordinary kinetic stabilities in oxidizing environments. From the time of Schonbein and Faraday (1830s), the reason for this stability has been attributed to the existence of a thin reaction product film on the metal (or alloy) surface. This film effectively isolates the metal from the corrosive environment. However, attempts to elucidate the mechanisms of the formation of passive oxide films, which generally comprise bilayer structures consisting of a defective oxide that grows directly into the metal and an outer, precipitated hydroxide (or oxyhydroxide on even oxide) layer, have yielded only a rudimentary understanding of the chemistry and physics of the growth and breakdown processes. In this paper, selected aspects of passivity and passivity breakdown are reviewed, with emphasis on the physical models that have been proposed to account for the experimental observations. One such model, the Point Defect Model, is shown to account for most, if not all, experimental observations, and to provide a robust basis for predicting the occurrence of passivity breakdown in any given system. By combining the Point Defect Model with deterministic models for pit growth and crack growth, it is now possible to predict the evolution of localized corrosion damage in a wide range of systems.

INTRODUCTION

A discussion of the passivity of metals in not inappropriate for the 7th International Chemistry Conference in Africa, because it is probable that humankind's first use of metals occurred on the African continent. Although much argument exists as to when this occurred, it is likely that some metals were used several tens of thousands of years ago, well before recorded human history. These metals were almost certainly the native metals; that is, those that are found in nature in the metallic form, including copper, silver, and gold. Much later, humans learned to smelt ores and formulate alloys (the 'Bronze Age', 4000–2000 BC), including the smelting of iron (the 'iron age', starting more than 2000 years ago) resulting in unprecedented technological transformation of society. The mastering of iron and steel production resulted in the development of machines, which in turn led to the industrial revolution. Still later, more highly reactive metals that possess particular properties (e.g. low densities), principally aluminum, magnesium, titanium and zirconium, were obtained using electrochemical methods. These metals and their alloys ushered in technologies and systems as diverse as high performance aircraft and nuclear power. Along with fire, the wheel, and the derivation of language, the development of metals and alloys has been a cornerstone in the evolution of the human experience.

Our modern industrial society is built upon the reactive metals; that is on those metals that react spontaneously with oxygen or water under terrestrial environmental conditions. These metals include (but are not limited to) Fe, Ni, Cr, Zn, Al, Ti, Pb, Mg, U, Be, Sn and W, all of which occur in nature in an oxidized form and hence all of which must be recovered by reduction. As noted above, these metals react

*Lecture presented at the 7th International Chemistry Conference in Africa & 34th Convention of the South African Chemical Institute, Durban, South Africa, 6–10 July 1998, pp. 919–1024.

with water and/or oxygen and many possess energy densities that are comparable with those of common fuels. For example, the energy densities of Al, Be, Mg and Zn in their reactions with oxygen under standard conditions are 21 994 W.h/kg, 33 151 W.h/kg, 6859 W.h/kg, and 9677 W.h/kg, respectively, compared with 9741 W.h/kg for decane (a simulant for gasoline). The high-energy content of aluminum, for example, is witnessed by the fact that powdered aluminum is used to boost the energy density of solid rocket fuels.

How is it possible, then, that our metals-based civilization could be based on the reactive metals? The answer to this question lies in the remarkable phenomenon of 'passivity' [1–9] that apparently was first defined by Keir in 1790. This phenomenon, which results in the kinetic stability of reactive metals, was explored extensively by Schonbein and Faraday 40 years later (i.e. more than 160 years ago, see the brief history of passivity given by Uhlig in [3]). Schonbein apparently coined the word 'passivity', but it was Faraday, on the basis of his famous iron-in-nitric acid experiment, in which iron was found to be immune from attack in concentrated nitric acid but not in dilute nitric acid, who brought the phenomenon to the forefront of electrochemistry [3]. This observation was not fully understood until the development of the electrochemical thermodynamic diagrams by Pourbaix in the 1960s [10] and it is still misinterpreted by many people. In any event, the reactive metals may be used only because of the formation of thin reaction product layers ('passive films') on the surface that effectively protect the underlying metal from the corrosive environment.

The phenomenon of passivity is best illustrated, in modern form, by reference to the current–voltage or 'polarization' behavior, as shown in Fig. 1 for iron in phosphoric acid/phosphate buffer solutions [2]. On increasing the voltage from the left side of the figure in the positive direction, the current at first increases more-or-less exponentially in the 'active' region, where the predominant reaction is metal dissolution. At a sufficiently high voltage, after passing through a maximum, the current decreases to a plateau that defines the passive state. For iron in this particular medium, the passive state exists over a voltage range of about 1 V, which may be compared with the voltage range of 1.23 V for the thermodynamic

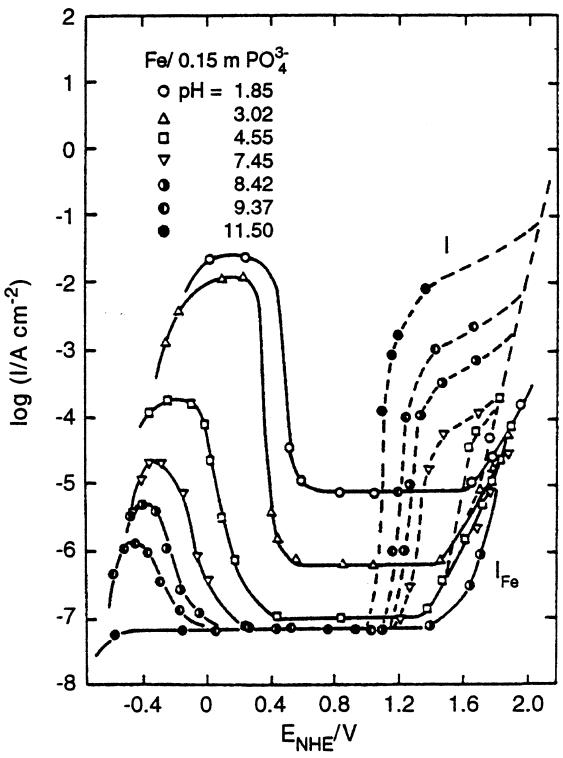

Fig. 1 Anodic polarization curves for iron in 0.15 M Na_3PO_4/NaOH solutions of different pH values showing the dissolution current, I_{Fe} (solid curves) and the total current, I (dashed curves) after 1 h in the steady state. After Sato [2].

stability of water ($p_{H2} = p_{O2} = 1$ atm) at 25 °C. At still higher voltages, the current again increases due to oxygen evolution. The data of Sato [2], shown in Fig. 1, reveal that oxygen evolution (which dominates the dashed curves) becomes increasingly prevalent at lower voltages as the pH increases. This effect primarily reflects the shift in the equilibrium voltage for the oxygen electrode reaction. Also to be noted is the fact that the dissolution current remains constant well into the oxygen evolution region, but that it ultimately increases at a sufficiently high voltage. Although considerable argument exists as to the mechanism of transpassive 'dissolution', one possibility is that the passive film breaks down over extended regions of the surface, rather than at localized points as in the case of pitting [1]. This is expected to occur if cation ejection from the barrier layer involves a change in the oxidation state of the ion (e.g. $Fe^{2+} \rightarrow Fe^{3+} + V_{Fe} + e^-$), thereby generating cation vacancies (V_{Fe}) in a charge transfer process. If the potential is sufficiently high, the rate of generation of cation vacancies at the bl/ol interface, and hence the flux of cation vacancies across the barrier layer, becomes insensitive to local structural variations. Under these circumstances, cation vacancy condensation will occur over extended regions. Regardless of the exact mechanism, transpassive dissolution marks the upper boundary of the passive state.

As noted above, the nature of passivity and the structure of the passive layer have been the subjects of intense curiosity for 170 years. However, it wasn't until the development of various electron microscopies (e.g. SEM, TEM) and *in situ* techniques, such as ellipsometry and more recently STM (Scanning Tunneling Microscopy) and AFM (Atomic Force Microscopy), that researchers have been able to construct physical/morphological models. The general picture that has emerged [1] is that the passive film forms as a bilayer structure comprising a defective oxide layer (the 'primary' passive film) that forms directly from the metal and a precipitated outer layer that forms via the hydrolysis of cations ejected from the inner layer, as depicted schematically in Fig. 2.

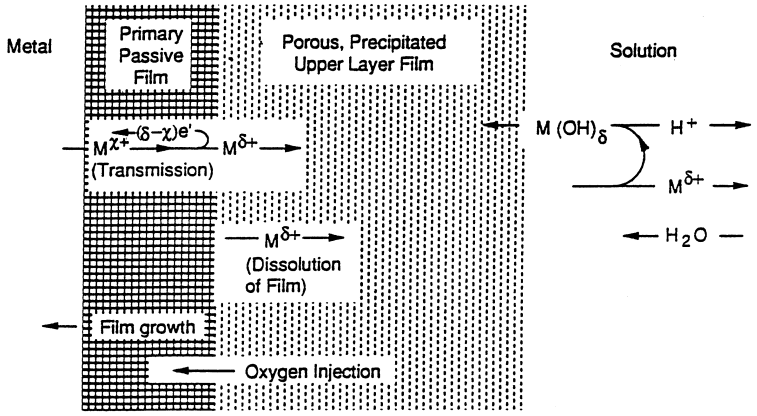

Fig. 2 Schematic of processes that lead to the formation of bilayer passive films on metal surfaces.

The goal of this paper is to review some of the physico-electrochemical aspects of passivity, including the mechanisms of growth and breakdown of the passive film. This is done primarily within the framework of the Point Defect Model [1], which has been developed by the author and his co-workers over the past 20 years to provide a mechanism-based description of the growth and breakdown processes. Other aspects of passivity and passivity breakdown have been reviewed extensively elsewhere [2–8], and the reader is referred to those sources for additional information.

THE PASSIVE STATE

Faraday's paradox

In Faraday's iron-in-nitric acid experiment, which he reported in 1836 (cited in [3,9]), it was reported that iron freely corrodes in dilute nitric acid with the evolution of a gas (hydrogen). However, in concentrated nitric acid, no reaction apparently occurred, in spite of the greater acidity of the medium ('pH' was an unknown concept in the 1800s). If the surface was scratched *in situ*, a burst of corrosion activity occurred

along the scratch, but then quickly died away. Faraday correctly surmised that the surface had become 'oxidized', yet the oxide film was too thin (order of a few nanometers) to be detected by the naked eye (thicker films would have produced interference patterns, the physics of which were more-or-less known since the time of Newton and Huygens). The intriguing question arose, then, as to why the surface became 'passive' in the more aggressive environment, contrary to the expectations at the time of the experiment. The answer to this paradox was not to evolve for more than 130 years.

In the 1960s, electrochemistry underwent a profound transformation with the introduction by Marcel Pourbaix [10] of his 'potential-pH diagrams.' In his *Atlas of Electrochemical Equilibria*, Pourbaix summarized the electrochemical thermodynamic behaviors of most of the elements in the periodic table. Subsequently, Pourbaix diagrams have been derived for many metals in complex environments (e.g. $Cu/NH_3/CO_2/H_2O$) and in environments under extreme conditions (e.g. Fe/H_2O at supercritical temperatures of $T > 374.15\,^{\circ}C$). For our purposes, only a simple, schematic diagram for the iron-water system is needed to illustrate the solution to Faraday's paradox. With reference to Fig. 3, and noting that for spontaneity the Second Law of Thermodynamics requires that

$$(E - E^e)I \geq 0 \tag{1}$$

where E is the potential, E^e is the equilibrium potential, and I is the current for the cell SHE/R/O, we see that the corrosion potential must satisfy the relationship $E_a{}^e < E_{corr} < E_c{}^e$. The current I is defined as being positive for a reaction that occurs in the oxidation sense and as negative for a reaction that occurs in the reduction sense. The potentials $E_a{}^e$ and $E_c{}^e$ refers to the equilibrium potentials for the partial anodic and cathodic reactions, respectively, in the corrosion process. Thus, iron in deaerated acid solution, in which the partial anodic and cathodic reactions are $Fe \rightarrow Fe^{2+} + 2e^-$ (Reaction (1), Fig. 3) and $H^+ + e^- \rightarrow \frac{1}{2}H_2$ (Reaction (a) Fig. 3), respectively, will adopt a corrosion potential that lies between Lines 1 and *a*, with the value of E_{corr} being determined by the relative values of the kinetic parameters of the two

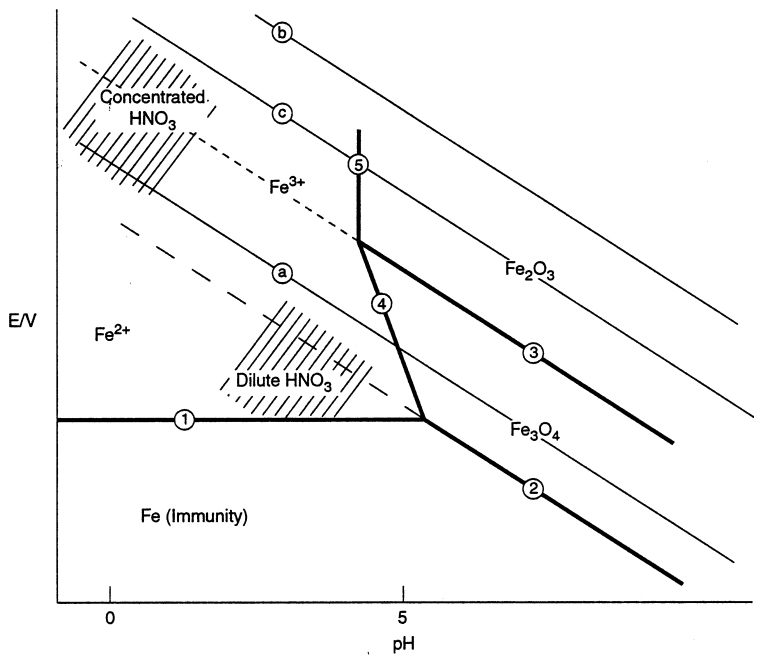

Fig. 3 Schematic Pourbaix diagram for iron illustrating the resolution of the Faraday paradox in the corrosion of iron in nitric acid. Lines (a) (b), and (c) correspond to the equilibria:

$H^+ + e^- \rightleftharpoons \frac{1}{2}H_2$ (a)

$O_2 + 4H^+ + 4e^- \rightleftharpoons 2H_2O$ (b)

and

$NO + 3H^+ + 2e^- \rightleftharpoons HNO_2 + H_2O$ (c)

respectively.

partial processes. In oxygenated (aerated) solutions, E_{corr} may lie between Lines 1 and b, because the reduction of oxygen is a possible (likely) cathodic reaction.

Faraday, as far as we know, did not have a reference electrode or a high impedance voltmeter, so that he could not have known where on Fig. 3 (which did not exist at that time) the corrosion potentials for iron in dilute nitric acid and in concentrated nitric acid lay. However, from 160 years of collective experience in electrochemistry, since the time of Faraday, we may speculate on the E/pH conditions that existed in his experiments, as shown in Fig. 3. Dilute HNO_3 is only a weak oxidizing agent, so that the principal cathodic reaction was most likely hydrogen evolution, and hence the corrosion potential is expected to lie between Lines 1 and *a* at relatively high pH, as indicated. On the other hand, concentrated HNO_3 is a strong oxidizing agent due to the reaction

$$NO_3^- + 3H^+ + 2e^- \rightleftarrows HNO_2 + H_2O \quad (2)$$

so that E_{corr} can lie anywhere between Lines 1 and c at low pH. Now, the Fe/Fe^{2+} reaction is relatively fast compared with H^+/H_2 on iron. This results (from Mixed Potential Theory) in the corrosion potential lying below the extension of Line 2 (Fe/Fe_3O_4) into the Fe^{2+} stability field, but, of course, above Line 1, in the case of dilute HNO_3. Under these conditions, Fe_3O_4 cannot form on the surface, even as a metastable phase. Thus, iron is active (freely corrodes) in this medium. However, in the case of concentrated HNO_3, Reaction (2) is likely to be fast (if for no other reason than the high concentration of NO_3^-), so that the corrosion potential will be high and certainly will be more positive than the extension of Line 2 into the stability region for Fe^{2+} an low pH. Accordingly, Fe_3O_4 can form as a metastable phase, thus giving rise to passivity and hence to the observed kinetic inactivity of iron in this medium. Removal of the film by scratching would cause the local potential to drop, due to the sudden dissolution of iron, thereby rendering hydrogen evolution a viable cathodic reaction. However, depletion of H^+ at the scratch would eventually cause the potential to shift in the positive direction and lead to the reformation of Fe_3O_4 as a metastable, passivating phase. If the potential becomes sufficiently positive, it may even lie above the extension of Line 3. In this case, Fe_2O_3 may form on Fe_3O_4 as an additional metastable phase, resulting in the bilayer structure that is commonly observed [2].

Because Fe_3O_4 is metastable (in the case of concentrated HNO_3), its existence on the surface depends upon a balance between the rate of formation and the rate of removal. If one or both of these processes depends upon the thickness of the Fe_3O_4 layer, then a steady state in the thickness (and in the current) will be observed. Thus, although thermodynamics alone is sufficient to resolve Faraday's paradox, a satisfactory theory of the passive state requires a detailed description of the kinetics of growth of the passive film and in particular of the processes that occur at the metal/film and film/solution interfaces.

Film growth models

The properties of passive films that must be accounted for by any successful model or theory for the passive state are as follows:

1 Passive films form as bilayer structures, consisting of a defective oxide (the barrier layer) adjacent to the metal and an outer layer that forms from the reaction of metal cations with species in the solution (including the solvent). Solution phase species may be incorporated in the outer layer, but not in the inner layer, whereas alloying elements from the substrate alloy may be incorporated into both layers [1].

2 For systems were the outer layers does not form, or where the outer layer presents little impediment to transport of species to the barrier layer/outer layer (bl/ol) interface, the specific impedance in the absence of redox couples is very high ($\sim 10^6$–$10^7\ \Omega \cdot cm^2$ for NiO on Ni) but in the presence of a redox couple[e.g. $Fe(CN)_6^{3-/4-}$] the impedance is often low [1]. This demonstrates that the barrier layers may be a good electronic conductor but generally is a poor ionic conductor.

3 Given sufficient time, steady states are observed in the barrier layer thickness and in the current. While this point is still somewhat controversial, steady states have been demonstrated unequivocally for Ni [11], Zn [12], and W [11], amongst other metals.

4 Provided that no change occurs in the cation oxidation state with distance through the barrier layer

phase, then the steady-state thickness varies linearly with the applied voltage. The logarithm of the current is also found to vary linearly with voltage, with a positive, finite slope being predicted, and observed, if the barrier layer is a cation conductor (e.g. NiO/Ni [11]). On the other hand, $\ln(I_{ss})$ vs. E has a zero slope if the barrier layer is an interstitial cation conductor (ZnO/Zn [12]) or an anion conductor (WO_3/W [11]), but only if no change in oxidation state occurs on the ejection of a cation from the barrier layer [1].

5 Metals possessing low oxidation states in the barrier layer tend to form cation-conducting (e.g. NiO/Ni) [11] or cation interstitial-conducting (ZnO/Zn) [12] barrier layers, while metals possessing high oxidation states form anion-conducting barrier layers (e.g. WO_3/W and ZrO_2/Zr) [1].

6 Cation vacancy conducting barrier layers tend to be p-type in their electronic character[e.g. NiO/Ni [11]), while those that are cation interstitial conductors (e.g. ZnO/Zn [12]) or anion conductors (W/WO_3 [11]) are *n*-type.

While these six generalizations are not all encompassing, in that others may exist, they are sufficient to differentiate between various theories that have been proposed for the growth of barrier oxide layers on metals and alloys. Six models that have been developed to describe the growth of anodic oxide films on metals are listed in Table 1, together with some of their important features and predictions. Of the six models listed, which were chosen because they make analytical predictions that can be tested, only the Point Defect Model (PDM) in its modified form [1,11] accounts for all of the observations summarized above. The original PDM [19], which ignored the dissolution of the barrier layer, and which did not differentiate the interfacial reactions on the basis of lattice conservancy, did not predict steady-states in the current or barrier layer thickness. Steady-states in the current and barrier layer thickness are also not predicted by the Verwey [13], Cabrera & Mott [14], and Sato & Cohen [16] models, and hence these models, too, must be discarded. Furthermore, a recent analysis of potentiostatic transients [20] demonstrated that the 'high field' models [13,14] are incapable of fully describing the kinetics of film growth on metals that form anion (oxygen) conducting passive films (e.g. Zr, W, Ta). This analysis [20] was a test of the electric field/thickness relationship, and the experimental data were found to be consistent with an applied voltage-independent field, rather than with the an unconstrained field that is proposed for the high field models and other models (e.g. Kirchheim [17]) under potentiostatic conditions. A thickness-independent electric field strength, as embodied in the PDM, arises from the reasonable postulate that the field must be limited in its upper value by precursors to dielectric breakdown [1]. The most important such process is probably band-to-band (Esaki) tunneling, which produces a counter field that buffers the applied field [1]. In the case of the PDM, as the film thickens under potentiostatic transient conditions, the voltage drop across the metal/barrier layer interface decreases. This, in turn, reduces the driving force for injection of cations from the metal into the film and for the generation of oxygen vacancies, which leads to the formation of new film. Because the HFMs do not recognize the existence of potential drops at phase boundaries, the entire potential drop in these models must be accommodated across the film, sometimes leading to calculated field strengths that are significantly higher than the dielectric strengths of even the nondefective, bulk oxides.

An attempt has been made to modify the HFM by incorporating dissolution at the film/solution interface [18]. This modification yields steady states in the current density and film thickness, but it does not account for the voltage- and pH-dependencies of these quantities.

The basis of the PDM is illustrated in Fig. 4. Briefly, the barrier layer is viewed as being a highly defective, defect semiconductor in which the vacancies act as the electronic dopants. The vacancies generated and annihilated at the interfaces, which are normally separated by no more than a few nanometers. Under anodic polarization conditions, there exists a net flow of oxygen vacancies from the m/bl interface (at $x = L$) to the bl/ol interface (at $x = 0$) and a net flow of cation vacancies in the reverse direction. Of the utmost importance in developing an understanding of the growth of the barrier-layer, is the differentiation of the interfacial reactions as to whether they are lattice conservative or nonconservative processes. Thus, Reactions (1) (3), and (4) in Fig. 4 are lattice conservative, because their occurrence does not result in the movement of the boundary with respect to the laboratory frame of reference. On the other hand, Reactions (2) and (5) generate and destroy the barrier layer, respectively, so that these processes are lattice nonconservative. The steady-state exists when the rates of these two

Table 1 Comparison of film growth models

Model	Applicability	Field strength	Rate control	Film dissolution	Interfacial pot. diff.	Electronic structure	Predictions
Verwey [13]	Cation conductors	Unconstrained	Cation motion in oxide	No	No	Not addressed	$i(t)$, L(t)
Cabrera-Mott [14]	Cation conductors	Unconstrained	Cation injection from metal into film	No	No	Not addressed	$i(t)$, L(t)
Vetter & Gorn [15]	Iron	Unconstrained	Cation ejection	Partly	Yes	Not addressed	$i(t)$
Place exchange [16]	Cation/anion conductors	Unconstrained	(i) Cooperative cation/anion exchange [ ] (ii) Injection of O^{2-} into the film	No	No	Not addressed	$i(t)$, L(t)
Kirchheim [17]	Iron	Unconstrained	Unclear	Yes	Yes	Not addressed	L_{ss}, L_{ss}, $i(t)$, L(t)
Point defect [1]	Cation/interstitial/ anion conductors	Constrained by Esaki tunneling	Cation injection from metal	Yes	Yes	Highly doped (degenerate) defect semi-conductor	Z(jw), alloy segregation, passivity breakdown

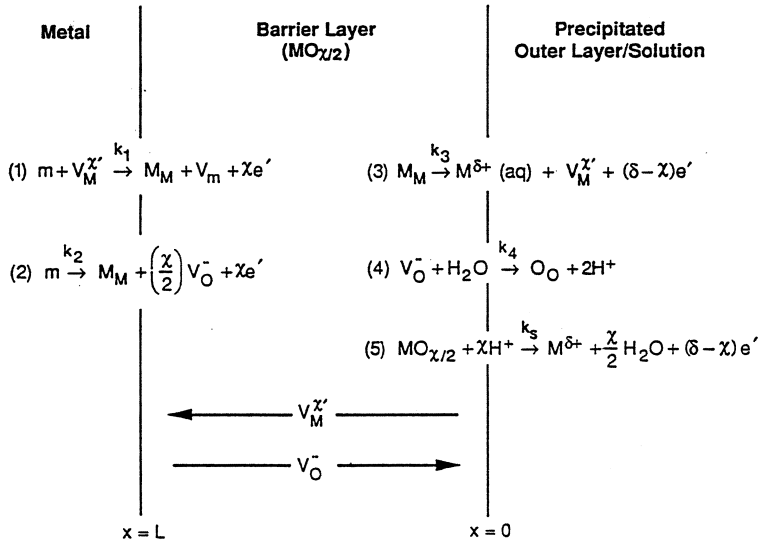

Fig. 4 Schematic of physico-chemical processes that occur within a passive film according to the point defect model. m = metal atom, M_M = metal cation in cation site, O_O = oxygen ion in anion site, $V_M^{\chi'}$ = cation vacancy, $V_O^{\cdot\cdot}$ = anion vacancy, V_M = vacancy in metal phase. During film growth, cation vacancies are produced at the film/solution interface, but are consumed at the metal/film interface. Likewise, anion vacancies are formed at the metal/film interface, but are consumed at the film/solution interface. Consequently, the fluxes of cation vacancies and anion vacancies are in the directions indicated. Note that Reactions (1) (3) and (4) are lattice conservative processes, whereas Reactions (2) and (5) are not.

nonconservative processes are equal, leading to the following expressions for the steady–state barrier layer thickness (L_{ss}) and current density (I_{ss}) [11]

$$L_{ss} = \frac{1}{\varepsilon}\left[1 - \alpha - \frac{\alpha\alpha_d}{\alpha_2}\left(\frac{\delta}{\chi} - 1\right)\right]V + \frac{1}{\varepsilon}\left\{\frac{2.303n}{\alpha_2\chi\gamma} - \beta\left[\frac{\alpha_d}{\alpha_2}\left(\frac{\delta}{\chi} - 1\right) + 1\right]\right\}pH + \frac{1}{\alpha_2\chi K}\ln\left(\frac{k_2^0}{k_s^0}\right) \quad (3)$$

and

$$I_{ss} = \delta F\left[k_3^0 e^{\alpha_3\alpha\gamma V} e^{\alpha_3\beta\gamma pH} + k_s^0 e^{\alpha_d\alpha(\delta-\chi)\gamma V} e^{\beta\alpha_d(\delta-\chi)\gamma pH} \cdot c_{H^+}^n\right] \quad (4)$$

respectively. In these expressions, α is the polarizeability of the bl/ol ('film/solution') interface, α_j and k_j^0 are the transfer coefficient and standard rate constant for the j-th interfacial reaction depicted in Fig. 4, $\gamma = F/RT$, $K = \epsilon\gamma$, ϵ is the electric field strength, n is the kinetic order of the barrier layer dissolution reaction with respect to the concentration of H^+, α_d is the transfer coefficient for film dissolution, β is the dependence of the potential drop across the bl/ol interface on pH, and χ and δ are the cation oxidation states in the barrier layer and solution, respectively.

Equation 3 predicts that in the steady–state, the barrier layer thickness will vary linearly with the applied voltage, which is a ubiquitous relationship in the anodic oxidation of metals. Of particular importance is the last term, which states that ultimately, the thickness of the barrier layer is determined by the ratio of the standard rate constants for film formation (k_2^0) and film destruction (k_S^0). Equation 4 predicts that the steady-state current density consists of two terms; that for cation conduction (first term) and that for anion conduction. This latter term is written in terms of the equivalent rate of dissolution of the barrier layer (note that the flux of oxygen vacancies and the dissolution rate are related in the steady-state [1]). For many cases, $\delta = \chi$(e.g. NiO/Ni, WO_3/W), in which case the second term is independent of voltage for a constant pH [11]. Indeed, Equations 3 and 4 have led to the formulation of diagnostic criteria, which have been used to identify the barrier layer on nickel as being a cation conductor and that on tungsten as being an oxygen vacancy conductor [11]. Later, the analysis was extended to interstitial cation conductors, and it was found that the barrier layer on zinc is consistent with this type of conduction [12].

At this point, it is worth inquiring as to what determines the conduction type of a barrier layer. While a complete answer to this question has yet to be developed, a simple argument based on the Born model for

a charge-in-a-dielectric resolves many of the important issues, at least in a semiquantitative sense. Thus, the energy of formation of a vacancy of charge χ can be written as $\chi^2 e^2/\epsilon_0\epsilon_f$ r, where r is the vacancy radius, e is the electronic charge, ϵ_f is the dielectric constant, and ϵ_0 is the permitivity of the vacuum. Ignoring the difference in radii, it is evident that the ratio of the concentrations of cation vacancies to oxygen vacancies in an oxide varies with exp $[\chi^2/4]$, assuming that the species concentrations obey Boltzmann statistics. Accordingly, cation vacancies become disfavored relative to oxygen vacancies as χ increases, thereby rationalizing why the barrier layers on high oxidation state metals, such as Ti, Zr, Ta, and W, in the steady state, are predominantly oxygen ion (vacancy) conductors, while that on nickel is predominantly a cation conductor [11]. It must be emphasized, however, that this argument is not entirely satisfactory, because the barrier layer exists in a state that is far from equilibrium, due to the generation and annihilation of vacancies at interfaces that are frequently separated by no more than a few nanometers.

The final matter that will be addressed here, with regards to steady-state films, concerns the electronic structures of barrier layers. That they are semiconductors is not in doubt, but the current evidence is that they cannot be modeled as classical, weakly doped semiconductors, at least those that form on the pure metals. Thus Mott-Schottky analyses of the passive films on many metals reveal dopant levels of 10^{20}–10^{21}cm^{-3}, which are generally unattainable in the bulk oxides, and which is sufficiently high that degeneracy may be an issue. Furthermore, the dopant level is voltage dependent [18], with the level decreasing with increasing applied voltage for oxygen vacant films (e.g. WO_3 on W, Fig. 5). As noted above, there exists a correlation of high fidelity between the crystallographic defect type (as established by the electrochemical diagnostic criteria given in [11]) and the electronic defect type (obtained from Mott–Schottkey analysis and photoelectrochemical studies), which leaves little doubt that the dopants are the defects themselves. Given that multiple crystallographic defects may be present simultaneously in a barrier layer, and that the concentration of each defect is a function of distance through the film and of the applied voltage, it is to be expected that some systems may exhibit an electronic defect type that changes with potential, as has been found in the case of copper [30]. The picture that emerges [1] is that the barrier layer is a highly (and possibly, degenerately) doped defect semiconductor junction, with structures that

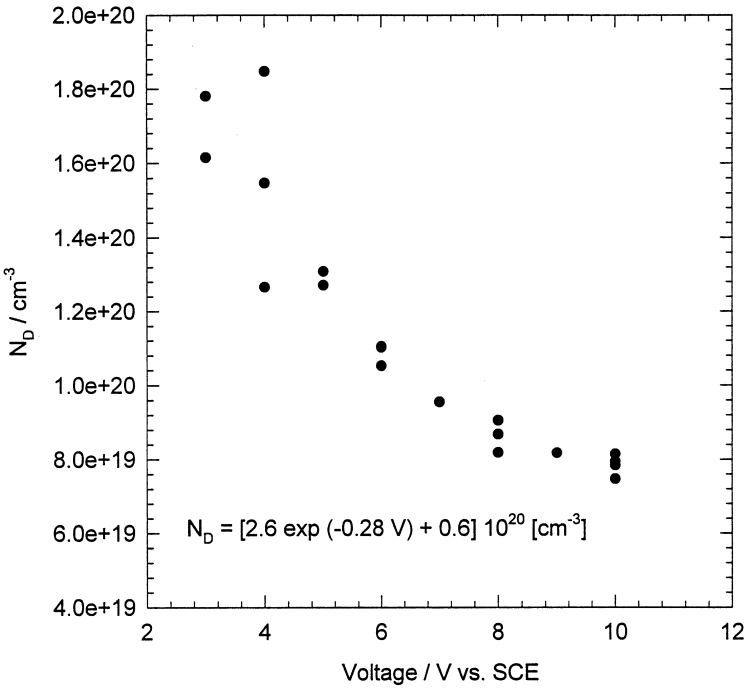

Fig. 5 Donor (oxygen vacancy) concentration in the passive film on tungsten as a function of formation voltage [18].

can best be described as m/n -*i* p_M^+/solution (for NiO/Ni), m/n_0^+-*i* - p_M/solution (e.g. WO_3/W), and m/n_i^+, n_0 -*i* - p_M/solution (ZnO/Zn) junctions, where p_M, n_0, and n_i represent cation vacancies, oxygen vacancies, and metal interstitials, respectively, in the film [1]. The superscript '+' represents dopant levels that are sufficiently high to induce degeneracy (i.e. to displace the Fermi level outside of the gap). Although detailed analyses of the electronic structures of barrier oxide layers have yet to be reported, it would seem that the closest classical analogs might be tunnel diodes [1]. That passivating oxide films are different from the bulk oxides was emphasized a century or so ago by Hittorf in his work on chemically passivated chromium, as noted by Glasstone [9].

The recent demonstration [20] that the classical theories for film growth are deficient, because of the incompatibility between experiment and theory with regards to the relationship between the electric field strength and the barrier layer thickness, has led to a reformulation of the growth laws for passive films. Thus, with reference to Fig. 4, we may write the change of the barrier layer thickness in terms of the rates of the two lattice nonconservative reactions as

$$\frac{dL}{dt} = -\frac{2\Omega}{\chi} J_O - \Omega k_s c_{H^+}^n \tag{5}$$

where Ω is the volume of the barrier layer per mole of cation, J_O is the oxygen vacancy flux at the metal/bl interface [due to Reaction (2), Fig. 4], and the last term describes the dissolution of the barrier layer via Reaction (5). Note that in the coordinate system used, J_O is a negative quantity. Electrochemical kinetic considerations show that $2J_O/\chi = -k_2$, where k_2 is the rate constant for the oxygen vacancy generation reaction, and that

$$k_2 = k_2^0 e^{a_2 V} e^{-b_2 L} \tag{6}$$

In this expression, $a_2 = \alpha_2 (1 - \alpha)\gamma$, $b_2 = \alpha_2 \chi \epsilon \gamma$, $\gamma = F/RT$, V is the applied voltage, L is the barrier layer thickness, and k_2^0 is the standard rate constant for Reaction (2), Fig. 4. Thus, for potentiostatic conditions

$$\frac{dL}{dt} = a e^{-b_2 L} - c \tag{7}$$

where

$$a = \Omega k_2^0 e^{a_2 V} \quad \text{and} \quad c = \Omega k_s C_{H^+}^n.$$

If the rate of dissolution is negligible, either because it is inherently so or because the bl/ol interface is screened by the outer layer, the change in *barrier* layer thickness can be integrated to yield

$$L(t) = \ln[e^{b_2 L_0} + a b_2 t]/b_2 \tag{8}$$

For $L_0 = 0$ and $ab_2 t >> 1$, Equation 8 collapses to the classical logarithmic growth relationship. A plot of Equation 8 is shown in Fig. 6, in comparison with L(t) calculated from the classical high field mechanism [20]. The differences between the two are not remarkable, emphasizing the difficulty in employing the integrated rate expressions for differentiating mechanisms, particularly if the initial thickness, L_0, is unknown. For c being independent of *t* and hence of L, Equation 7 is readily integrated to yield

$$\ln\left[\frac{e^{-b_2 L}(c - a e^{-b_2 L_0})}{e^{-b_2 L_0}(c - a e^{-b_2 L})}\right] = b_2 c t \tag{9}$$

Expansion of the left-hand side yields a slightly different form as

$$L = L_0 + \{\ln[1 - (a/c)e^{-b_2 L_0}(1 - e^{b_2 c t})]\}/b_2 - ct \tag{10}$$

which appears to be the most explicit form of L(t) that can be obtained. It is readily shown that as $t \rightarrow \infty$, $e^{-b2L} \rightarrow c/a$, which defines the steady-state [Equation 3]. No parametric analysis of Equation 9 has yet been reported, but it is the only growth law of which the author is aware that recognizes dissolution of the barrier layer.

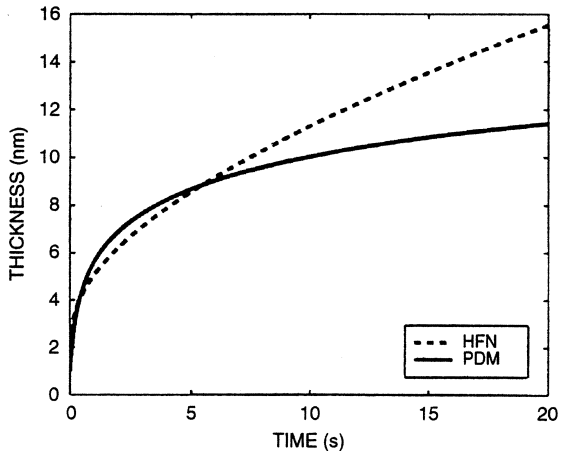

Fig. 6 Predicted growth of a passive film according to the HFM and the PDM as calculated using parameter values given in [20].

Finally, we note that putting $dL/dt = 0$ (steady state) yields Equation 3. Furthermore, if an outer, precipitated layer forms, whose porosity is time-dependent, then c may also be time-dependent, resulting in a deviation from the behavior predicted by Equation 9. A complete treatment of the kinetics of growth of bilayer oxide/hydroxide structures has yet to be reported, although an analysis of the bilayer structure that forms on lithium in contact with aqueous solutions, in which a LiH barrier layer is believed to form, has been accomplished [21].

PASSIVITY BREAKDOWN

While passivating oxide films greatly reduce the dissolution rates of metals (see Fig. 1), they do not completely protect the surfaces from corrosion. In particular, passive surfaces are susceptible to various forms of localized corrosion, including pitting corrosion, stress corrosion cracking, corrosion fatigue, and crevice corrosion. The occurrence of each of these phenomena requires the initial breakdown of passivity, in which the barrier layer is ruptured and the underlying metal is exposed to the environment. Provided that the breakdown event survives (generally about one chance in one hundred to ten thousand for type 304 stainless steel in chloride-containing solution [22]), propagation requires the continued separation of the anode and the cathode, such that an aggressive environment is maintained within the developing crevice. Subsequently, the crevice may repassivate, due to the evolution of the system to a state where separation of the anode and the cathode cannot be maintained, or because changes in the external environment interrupt the underlying mechanisms.

The experimental evidence

As the result of more than 70 years of intensive research on the causes of localized corrosion by many workers, it is possible to generalize the experimental findings as follows:

1 Localized corrosion occurs on a wide variety of passive metals and alloys in a wide variety of environments. However, certain species (e.g. Cl^- and Br^-) induce passivity breakdown by interacting with the barrier layer [1,3–6,23].

2 Passivity breakdown occurs at a wide variety of sites on metal and alloy surfaces, including ghost grain boundaries and projected dislocations, in the case of pure metals, to precipitates and inclusions in the case of alloys (e.g. MnS inclusions in the case of stainless steels [23]). Many of these sites are, themselves, nonreactive or at least only weakly reactive (e.g. Al_2Cu inclusions in Al alloys [4]), but they all represent structural and chemical discontinuities in the barrier layer.

3 Passivity breakdown is a dynamic phenomenon, in which transient breakdown/repassivation events occur over the large population of potential breakdown sites that exist on a real surface (metastable pitting). The statistical characteristics are quasi-Poissonian, leading many to conclude that passivity

breakdown is a stochastic (random) process [22,24,25]. However, certain sites on a surface are more prone to breakdown than are others, for well-established physico-chemical reasons (see later). Accordingly, passivity breakdown is fundamentally a deterministic process, with the outcome of the process (breakdown) being (in principle) predictable on the basis of known physical laws.

4 The transition of a metastable event to a stable event, and hence the nucleation of a stable pit, is a rare event [22], with the probability of occurrence being of the order of 10^{-2}–10^{-5} for many systems. The probability of survival is determined by the kinetics of repassivation, which depend on the chemical composition of the environment, on the nature of the breakdown sites, and on the electrochemical properties of the system. Two fundamentally different repassivation phenomena may be identified: (i) 'Prompt' repassivation of the postbreakdown event, in which the nucleus fails to achieve the threshold conditions necessary for survival [22,24,25], and (ii) 'delayed' repassivation, in which competition for the limited resources on the external surfaces (e.g. oxygen reduction) allows only the fittest pits to survive [26].

5 A single passivity breakdown event on a surface is characterized by a critical voltage (V_c) and induction time (t_{ind}), regardless of the ultimate fate of the nucleus. For an ensemble of events that characterize a real surface, V_c is found to be near-normally distributed while t_{ind} displays a left acute distribution [27]. The distribution in V_c is characterized by a well-defined mean value (i.e. $\bar{V}_c$) and by a well-defined dispersion.

6 The parameters V_c (and $\bar{V}_c$) and t_{ind} exhibit highly characteristic dependencies on the activities of the breakdown-inducing aggressive species (a_x) and applied voltage (t_{ind} only) for a wide variety of systems, suggesting commonality in mechanism [1]. These dependencies include V_c (or $\bar{V}_c$) $\propto -\log(a_x)$ and $\log(t_{ind}) \propto -\Delta V$ for small ΔV ($= V - V_c$), or $\log(t_{ind}) =$ constant for high ΔV [28].

7 V_c (and $\bar{V}_c$) are found to depend on the identity of the aggressive ion within a homologous series. For example, in the case of iron and stainless steel [1,4,23], the ability of a halide to induce passivity breakdown changes in the order $F^- < Cl^- > Br^- > I^-$. On the other hand, in the case of titanium, passivity breakdown is induced more readily by Br^- than by Cl^- or I^- [23,29]. The 'aggressiveness' of a halide is not just a matter of ion size, but it depends also on the thermodynamics of hydration and on the properties of the substrate [1]. In many cases, pits nucleate at sites for which there exists no rational mechanism of interaction with an aggressive anion like chloride, even though dependencies of V_c and t_{ind} on the ion activity are observed. For example, numerous authors have attributed pit nucleation on stainless steels to the dissolution of MnS inclusions, and there is little doubt that dissolution occurs. However, as noted above, there appears to be no rational, mechanism-based explanation, based on MnS dissolution, for the observed dependencies of V_c on ion (halide) size and on halide activity. Thus, one is forced to conclude that, while MnS dissolution is involved in the *propagation* of micropits, it is not the fundamental event that marks *initiation*.

8 In many systems (e.g. Al, Ga, Zr, stainless steel), blister formation is observed to be the precursor to passivity breakdown [1,29]. Remnants of the blisters (i.e. the 'cap') are believed to play a vital role in causing and maintaining a separation between the anode (within the cavity) and cathode (on the external surface) during the crucial, early stages of the growth of the nucleus [30].

9 Certain alloying elements, notably those with oxidation states greater than that of the host metal (e.g. Mo in Ni), when present in the barrier layer, cause a positive shift in V_c (and $\bar{V}_c$) and in a lengthening of the induction time [1,4,27]. The effect is greater for a larger difference in the oxidation states between the solute and host, other factors being the same (see later).

10 Incident electromagnetic radiation, with a photon energy that is greater than the bandgap of the barrier layer oxide, also results in a positive shift in V_c (and $\bar{V}_c$) and in a lengthening of the induction time [1,31–35]. This 'photoinhibition' of passivity breakdown (PIPB) effect has been found to occur on a variety of metals (Ni, Fe, Cu) and alloys (stainless steels, Cu-Ni alloys), and becomes stronger with increasing photon energy and with increasing photon flux (intensity) [34,35]. Finally, photoinhibition is considerably muted if the barrier layer is screened by the precipitated outer layer, at least in the case of stainless steels [34]. This observation demonstrates that the barrier layer is responsible for passivity and passivity breakdown, and that is the defect (electronic and crystallographic) structure of the barrier layer that is modified by irradiation.

Theories and models

Numerous theories and models have been proposed for passivity breakdown [1–6], but space does not allow them to be reviewed here. Only three of these theories are analytic, in the sense that they yield analytical relationships between measurable parameters and various independent variables that can be tested experimentally [1]. In particular, the Point Defect Model (PDM) of Lin, Chao, and of Macdonald [28] (later modified by Ellerbrock & Macdonald [28]) and the halide nucleus model of Okada [36] provide analytical expressions for both critical breakdown parameters (V_c, t_{ind}). Experimental evaluations of various theories and models by Lei *et al*. [37] and, in particular, by Milosev and co-workers [38] have shown that only the PDM is consistent with the experimental data for the systems investigated. Furthermore, the PDM accounts for the distributions in V_c and t_{ind}, for alloying effects, for photoinhibition of passivity breakdown, and for the evolution of localized corrosion damage [1]. Accordingly, the remainder of this paper reviews the PDM with only the occasional reference to other models. The exclusion of a detailed discussion of these other models is not meant to imply that they are unimportant, but it simply reflects the limitation of space.

The PDM postulates that passivity breakdown occurs as a result of cation vacancy condensation at the metal/bl interface at sites in the passive film that are characterized by high cation vacancy fluxes. These sites correspond to regions of structural discontinuity, such as (but not limited to) ghost grain boundaries, emergent dislocations, and the points of intersection between the barrier layer and precipitates (e.g. Al_2Cu in Al), inclusions (e.g. MnS in stainless steels), and other second phase particles. Two fundamental processes have been postulated as being responsible for passivity breakdown, both leading to an enhancement of the cation vacancy flux across the barrier layer in response to the absorption of aggressive anions into oxygen vacancies at the bl/ol interface (Fig. 7). Both mechanisms (Schottky pair generation

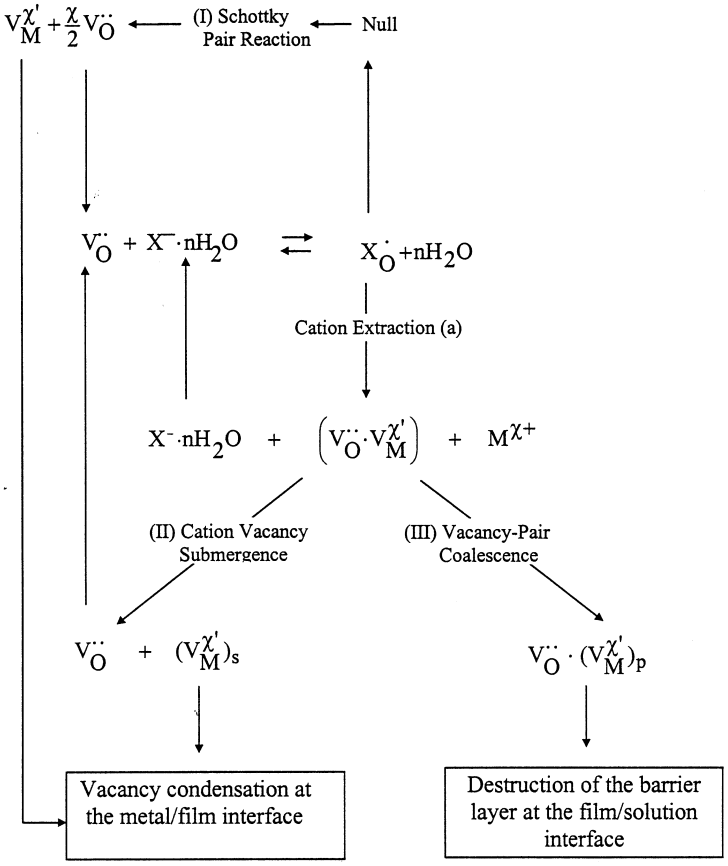

Fig. 7 Summary of proposed reactions leading to cation vacancy condensation at the m/bl interface and hence to passivity breakdown.

and cation extraction) give rise to the same expressions for the breakdown voltage and induction time, and both (most importantly) lead to the autocatalytic generation of oxygen vacancies at the bl/ol interface above the point of cation vacancy condensation.

The processes that are envisioned to occur during passivity breakdown are shown in the cartoon given in Fig. 8 [1]. The essential concept is that, if the enhanced flux of cation vacancies that occurs across the barrier layers is such that the vacancies cannot be annihilated by Reaction (1), Fig. 4 (the rate constant of which in the steady-state does not depend on the applied voltage), the excess vacancies condense at the periphery of an expanding condensate. This results in separation of the barrier layer from the metal, which prevents further penetration of the film above the condensate into the substrate, via Reaction (2), Fig. 4. However, at those regions beyond the condensate, where the barrier layer is still attached to the metal, the film continues to grow into the substrate. Simultaneously, dissolution of the barrier layer at the bl/ol interface results in the thinning of the cap over the expanding condensate, with the greatest extent of thinning occurring at the point at which vacancy condensation first occurred (because of the longest time since separation). Thinning of this type at precursor sites to pitting on stainless steels has been observed using microellipsometry [39]. Eventually, perforation of the 'cap' occurs leading to the penetration of electrolyte into the cavity (condensate) and hence marking the initiation of a micropit. The fate of the micropit is determined by the ability of the pit to achieve a critical size (or more correctly, a critical value of $i \cdot r$ or i/r, where i is the current density and r is the radius of the semispherical nucleus [22,24,25]). Failure to achieve these conditions, which are critically dependent upon the existence of the cap, at least in the early stages [22,30], is postulated to result in the passivation of the nucleus. This topic is discussed in greater depth later in this review.

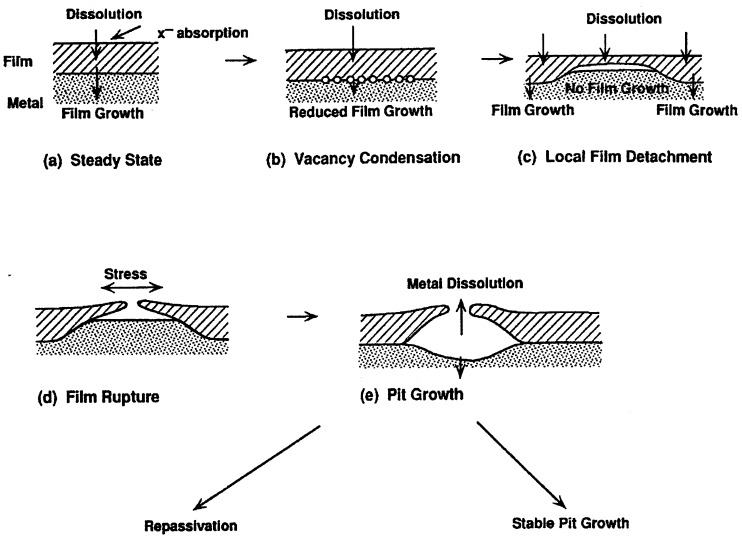

Fig. 8 Cartoon outlining various stages of pit nucleation according to the Point Defect Model.

The autocatalytic generation of oxygen vacancies at the bl/ol interface, as depicted in Fig. 7, is an important feature of the PDM. This is because it accounts for the intriguing observation of Bargeron and Givens [41,42] that rings of absorbed chloride exist at the peripheries of 'blisters' on the surface of aluminum in contact with chloride-containing solutions under spontaneous pitting conditions. The chloride ring expands with the blister, signaling a continual redistribution of absorbed chloride ion on the surface. This observation is in complete accord with the predictions of the PDM, because of the close spatial relationship between oxygen vacancy generation and cation vacancy condensation. Thus, the oxygen vacancy concentration at the surface, and hence the concentration of absorbed chloride, is greatest above the location of vacancy condensation, which coincides with the periphery of the blister. The autocatalytic generation of oxygen vacancies, ensures continued condensation of cation vacancies at the periphery of the condensate and hence ensures the continued growth of the blister.

Cation vacancy condensation (separation of the barrier layer from the substrate metal) is postulated to

occur when the 'excess' cation vacancy flux multiplied by the time over which condensation occurs exceeds a critical value [28]:

$$(J_{ca} - J_m)(t - \tau) \geq \xi \tag{11}$$

where J_{ca} is the flux of cation vacancies across the barrier layer at the breakdown site, J_m is the annihilation flux (i.e. the rate of Reaction (1), Fig. 4), t is the time, τ is the cap dissolution time (see below), and ξ is the critical area concentration of vacancies. The critical breakdown voltage for a given site is that voltage at which breakdown occurs after an infinite time, i.e. when $J_{ca} = J_m$, which leads to [27]:

$$V_c = \frac{4.606RT}{\chi\alpha F}\log\left[\frac{J_m}{J^0 u^{-\chi/2}}\right] - \frac{2.303RT}{\alpha F}\log(a_x) \tag{12}$$

Substitution of this expression into Equation 11 yields the induction time for passivity breakdown as [28]:

$$t_{ind} = \xi'\left[\exp\left(\frac{\chi\alpha F\Delta V}{2RT}\right) - 1\right]^{-1} + \tau \tag{13}$$

where $\Delta V = V - V_c > 0$ (i.e. for $J_{ca} > J_m$). In these expressions, $J^\circ = \hat{a}D$, D is the cation vacancy diffusivity, â and u are constants that depend on the thermodynamic parameters for the absorption of the aggressive ion into an oxygen vacancy at the bl/ol interface, a_x is the activity of the aggressive ion at the bl/ol interface, and ξ' is a parameter that depends on the critical areal concentration of condensed vacancies, ξ [28].

Equations 12 and 13 have been found to describe passivity breakdown quantitatively in each of the systems that have been analyzed in sufficient depth to permit the discrimination between different mechanisms (to the author's knowledge). These systems include Fe/CI^-, Br^-, I^- [28], Ni/CI^- [37], and Cu/HCO_3^-, SO_4^{2-} [38], with 'quantitative agreement' being taken as the close agreement between the values of α obtained from Equations 12 and 13. Perhaps of equal importance is the fact that Equation 12 explains the ubiquitous observation that V_c varies linearly with $-\log(a_x)$, with a coefficient that exceeds 2.303RT/F (note that $\alpha < 1$). Furthermore, Equation 13 explains the form of $\log(t_{ind})$ vs. ΔV, which is a straight line (of negative slope $\chi\alpha F/2RT$) at small ΔV (but sufficiently large that the exponential >> 1), but in which $t_{ind} = \tau$ is a constant at large ΔV.

Recently [43], the potential sweep rate dependence of V_c has been used to derive the value of ξ (the areal concentration of condensed cation vacancies for the separation of the barrier layer from the metal) for Ni in buffered chloride-containing solution, and the value so obtained is in good agreement with that obtained from structural considerations. This is a particularly stringent test, because the parameters in the calculation are fairly well-defined. We will see later that these same expressions (Equations 12 and 13) explain other phenomena related to passivity breakdown, including alloying effects and photoinhibition, in terms of modifications to the cation vacancy diffusivity (D), the electric field strength (ϵ), and the vacancy structure.

In the original PDM [28], the parameter τ was identified as a 'relaxation time', which described the temporal and spatial response of the vacancy structure to the absorption of an aggressive anion into an oxygen vacancy at the bl/ol interface. However, upon reinterpreting [29] the data of Cassilas *et al.* [44] for passivity breakdown on titanium, it became evident that τ is also (and, perhaps, exclusively) determined by the time of dissolution of the cap to the point that the cover becomes mechanically unstable. Thus, τ can be defined as

$$\tau \leq \Delta L/\Omega k_s c_{H^+}^n \tag{14}$$

where ΔL is the thickness of the barrier layer over the condensate at the point at which cation vacancy condensation first occurs, and the denominator is the barrier layer dissolution rate. At sufficiently high overvoltages ($\Delta V = V - V_c$), where vacancy condensation occurs rapidly, $t_{ind} \sim \tau$ and, unless the rate of dissolution of the cap depends on X^-, τ should be independent of the concentration of the aggressive species in the solution, but should be a function of the pH. With regard to this latter parameter (pH), τ should decrease with decreasing pH for pH < pzc, but should decrease with increasing pH for pH > pzc, where pzc is the pH of zero charge [11]. For the case of iron in chloride solutions, τ shows slight dependencies on [Cl^-] and pH [28], but the dependencies are judged to be too small to be of mechanistic significance. Also, assuming that $\Delta L \sim 2$ nm, and noting that $\tau \sim 10$ s, the maximum dissolution rate

[equal sign in Equation 14] of the cap above the cation vacancy condensate is estimated to be ~ 0.2 nm/s. This value corresponds to a minimal corrosion rate (ignoring cation transmission through the film) of ~ 6 mm/year, which is much too high to be realistic for iron in neutral chloride solution. This probably reflects the fact that only partial dissolution is necessary to cause the residual stresses to induce rupture of the cap. Alternatively, dissolution may be highly nonuniform, giving rise to high local penetration rates through the cap. Once the cap has ruptured, however, dissolution may occur from both sides to yield patterns that reflect the properties of both the internal and external environments. Indeed, the latter is implied by the recent studies of Laycock *et al*. [30], who analyzed the 'lace-like' perforations in the caps over pits that form on stainless steels in chloride-containing solutions.

Ellerbrock & Macdonald [28] recently reanalyzed the experimental data of Casillas *et al*. [44] for passivity breakdown on titanium in bromide-containing solutions, as noted above. The maximum dissolution rate of the cap, as estimated from Equation 14, was about 1 nm every 1000 s, leading to an estimate of the passive current density (assuming predominant oxygen vacancy transmission) of ~ 3.8 μA/cm. This value was considered to be reasonable, given the fact that no allowance was made for surface roughness, and noting that Casillas *et al*. [43] did not report passive current densities for their experiments. In retrospect, this value is now also considered to be too large and hence to imply that the inequality in Equation 14 is more appropriate than the equal sign.

The PDM has been criticized as being too 'static', because passivity breakdown is well-known to be a dynamic phenomenon (as shown by the existence of 'metastable' pitting). In the author's opinion, this criticism results from a lack of understanding of what the PDM (as outlined above) attempts to accomplish. Thus, the model attempts to describe the initiation event, i.e. the event that leads to rupture of the passive film that subsequently results in the transient in current. That this must involve the physical rupture of the film is self-evident, and the view that somehow initiation is preceded by dissolution of the substrate must be rejected as 'getting the cart before the horse.'

As demonstrated by Shibata and co-workers [27], and later by Williams *et al*. [22,45], and others [46], the breakdown parameters are distributed with V_c being near-normally distributed and t_{ind} being described by a left-acute distribution. These workers have chosen to interpret their data in terms of stochastic models, which presuppose that breakdown is a random phenomenon. This is justified on the basis that the breakdown voltage for metastable events is 'normally' distributed, and hence is Poissonian in nature. The fallacy in this argument is that, while a random breakdown process is expected to yield a normal distribution in V_c, when sampled over many events, the converse is not true; that is, a normally distributed V_c does not necessarily mean that the event is random in nature. Thus, Wu *et al*. [46] recently demonstrated that a 'stochastic' process incorporating short-term 'memory' effects does indeed yield the experimentally observed near-normal distributions in V_c and left acute distribution in t_{ind}, even though the process is not strictly 'random'. (These workers were apparently unaware that the same distributions had been derived deterministically more than a decade earlier [47,48].)

Finally, stochastic models are phenomenological models, and, as such, they cannot provide a satisfactory account of the physico-electrochemistry of the fundamental events involved in passivity breakdown. For example, the nucleation rate (λ) is derived as a model parameter, but nowhere in the stochastic treatment is there a physical model for, or explanation of, the processes that lead to the observed rate and its dependencies on various independent variables. Until this is done, the stochastic models must be regarded as being inadequate and incomplete, and to offer little more than a description of the phenomenon itself. That passivity breakdown is deterministic in nature would also seem to be self-evident from the data obtained from the stochastic models themselves, which yield model parameters (λ, μ, or τ_c) as functions of potential, inclusion size, flow velocity, temperature, and so forth. Clearly, there dependencies must reflect underlying mechanisms, which imply a determinism that governs the behavior of the ensemble of events.

Accepting that the initial event in the nucleation of a micropit is passivity breakdown, and that V_c and t_{ind} describe the breakdown conditions for a given event, then we may inquire as to what parameter in the model is most appropriately distributed in describing the behavior of the population of sites on the surface. The two most likely candidates are the cation vacancy diffusivity (D) and the thickness of the barrier (L_{ss}). That L_{ss} varies across a real surface is well-known from microellipsometric studies [39], but

distributing this parameter would seem to affect only those instances where the induction time is dominated by the rate of dissolution of the cap (i.e. at high ΔV or for inherently thick films, such as those that form on the valve metals, such as Ti [44]). To describe the more general case, the cation vacancy diffusivity within the population of breakdown sites was assumed to be distributed normally about a mean ($\bar{D}$) with a standard deviation, σ_D. The resulting distributions in V_c and t_{ind} were then derived as [47,48]:

$$\frac{dN}{dV_c} = -\frac{\gamma' D}{\sqrt{2\Pi}\cdot\sigma_D} e^{-(D-\bar{D})^2}/2\sigma_D^2 \tag{15}$$

and

$$\frac{dN}{dt_{ind}} = \left[\frac{\xi u^{\chi/2}}{\sqrt{2\Pi}\cdot\sigma_D\cdot\hat{a}}\right] e^{-(D-\bar{D})^2/2\sigma_D^2} \cdot \frac{e^{-\gamma' V}}{a_x^{\chi/2}(t_{ind}-\tau)^2} \tag{16}$$

where $\gamma' = \chi\alpha F/2RT$, and the other parameters are as previously defined. Equations 15 and 16 have been found to account for the distributions in V_c and t_{ind}, as reported by Shibata *et al*. [27], and more recently by others [45,46], as show in Figs 9 and 10. Note that these same expressions are applicable [43], whether it is the 'external' distribution (many specimens, as employed by Shibata [27]) or the 'internal' distribution (single specimen as employed by Williams *et al*. [45]) that is sampled. Also note, that in calculating the distribution in t_{ind} (Fig. 10) from the fit shown in Fig. 9, only σ_D was allowed to

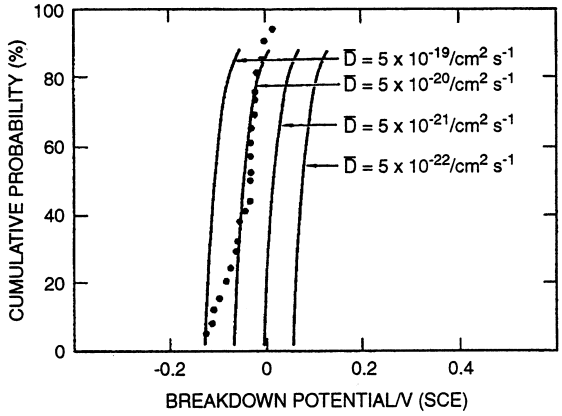

Fig. 9 Cumulative probabilities for the breakdown voltage as a function of $\bar{D}$ for normal distributions in the diffusivity D. $\sigma_D = 0.75$. Data for Fe-17Cr in 3.5% NaCl solution at 30 °C from Shibata [27]. See also [1,47]. $\bar{V}_c = -0.046$ V (SCE).

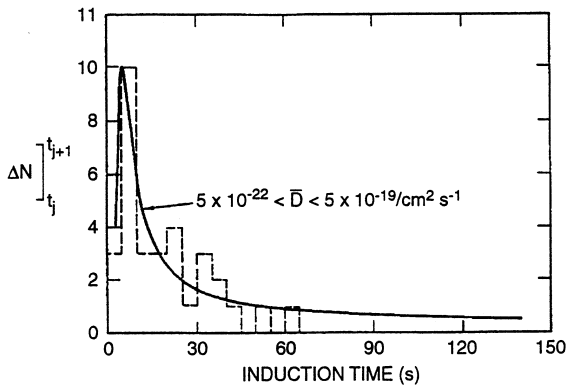

Fig. 10 Differential cumulative probabilities for the induction time as a function of $\bar{D}$ for normal distributions in D. $\sigma_D = 0.75\bar{D}$. (---) Data for Fe-17Cr in 3.5% NaCl solution at 30 °C from Shibata [27]. See also [1,47]. $\bar{V}_c = -0.046$ V (SCE), V = 0.020 V (SCE), t = 7.5 s, $\tau = 0$.

vary. However, the variation of this parameter did not significantly affect the shape of the distribution in t_{ind}, and the value that was adopted for the distribution in V_c was found to provide an accurate account of the induction time data [47,48]. In other words, there were no materially important adjustable parameters in calculating the distribution in t_{ind} from the fit of the model to $N(V_c)$.

The distributions in V_c and t_{ind}, as given by Equations 15 and 16, have been explored as a function of a_x, applied voltage ($N(t_{ind})$ only), and pH, with the expected dependencies being obtained [47,48]. Thus, while changes in $\log(a_x)$ induce only relatively small changes in $\bar{V}_c$ (see Equation 12, which also applies to the mean in $N(V_c)$), they have a large impact on $N(t_{ind})$, with t_{ind} being greatly decreases as a_x is increased. It is for this reason that passivity breakdown may be termed 'induction time-limited', although it is possible that this terminology should be discouraged, because $N(V_c)$ and $N(t_{ind})$ are not independent.

Equations 15 and 16 have led to the formulation of a theory for alloying. The basis of this theory is the Solute–Vacancy Interaction Model (SVIM) [49], which postulates that alloying elements that are substitutionally present in the cation sublattice of the barrier layer in an oxidation state that is higher than that of the host cation (e.g. Mo, where Mo is present as Mo(VI) in the NiO barrier layer) will interact electrostatically with the mobile cation vacancies, with the net result that the mean cation vacancy diffusivity is lowered. This has the result of shifting the breakdown voltage in the positive direction, to produce a more breakdown–resistant barrier layer. The SVIM has been applied to the Type 304 (18:8:Cr:Ni)/Type 316 (+ 2.5% Mo) issue, with the results of the calculation being shown in Fig. 11. The quantity that is plotted on the ordinate is $V(X) - V(X = 0)$, where X is the cation fraction of Mo in the film (assumed to be the same as that in the metal), eliminates all but one of the poorly known parameters in the model. The one remaining parameter that can have a profound impact on V_c and t_{ind} is the dielectric constant of the barrier layer, which was taken as being equal to that for the passive film on iron. While the experimental data are highly scattered, the PDM was found to best account for the effect of Mo by assuming that Mo exists in the +6 state, rather than in the +4 state.

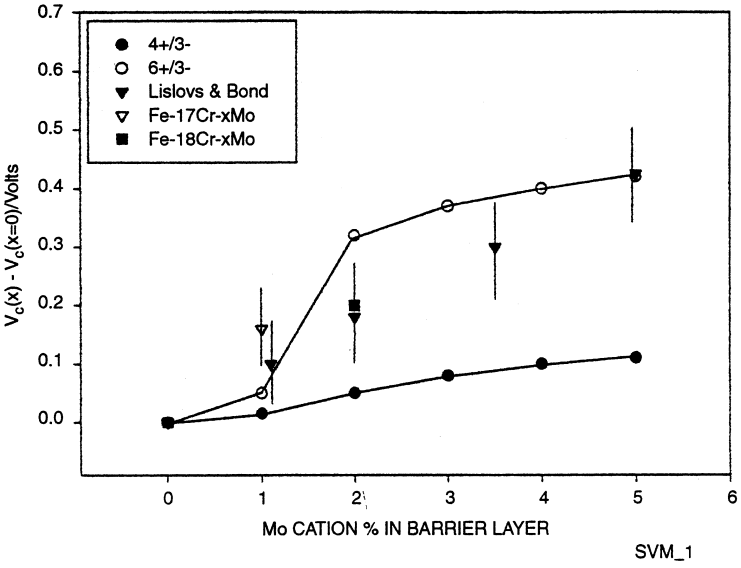

Fig. 11 Effect of molybdenum concentration on $\bar{V}_c(X) - \bar{V}_c(X = 0)$ for $6^+ - 3^-$ (o) and $4^+ - 3^-$ (●) complexes in the passive film on Fe-Cr-Ni-xMo alloys.
$n_v = 5 \times 10^{20}/cm^3$, $K_1 = 1.13 \times 10^{-16}$ cm^3 (○).
$K_1 = 1.13 \times 10^{-16}$ cm^3 (△).
▼ Lizlovs & Bond: Fe-18 Cr in 1 M NaCl at 25 °C.
▽ Shibata: Fe-17 Cr in 3.5% NaCl at 30 °C.
■ Shibata: Fe-18 Cr in 3.5% NaCl at 30 °C.
For other parameters and experimental data sources, see [1,49].

Another parameter that has a profound effect upon the breakdown parameters is the electric field strength. As pointed out earlier in this review, the electric field strength is buffered by electron/hole generation via band-to-band (Esaki) tunneling, which prevents the field from increasing in an unconstrained manner. However, if an additional $e'/h^{\cdot}$ generation process is imposed on the system, such as irradiation with super bandgap light, the field will be lowered, with the result that V_c is predicted to shift to more positive values and t_{ind} is predicted to increase to longer times. This is the basis of photoinhibition of passivity breakdown (PIPB), which was first reported by Lenhart *et al*. [31] for nickel in 1987 and then subsequently detected by various workers for iron [32,35], stainless steels [33,34], and copper alloys [50]. Recently, Shibata *et al*. [51] confirmed PIPB in stainless steel and analyzed their data in terms of a stochastic model. They found that the principal effect of super band-gap irradiation is on reducing the pit generation rate, which is precisely the effect predicted by the PDM (Equation 16).

Persistence in photoinhibition was first reported for iron by Schmuki & Bohni [32] and has been confirmed subsequently by Heaney & Macdonald [35]. Breslin *et al*. [34] have also demonstrated persistence of PIPB in stainless steels in chloride-containing solutions. In this persistent effect, the resistance to passivity breakdown induced by initial irradiation was found to remain for ≈ 250 h after irradiation had ceased, after which the system then returned to its initial, susceptible state. Schmuki and Bohni [32] explain persistence in terms of the generation of 'surface states' without specifying the nature of those states or how they are formed. On the other hand, persistence is readily accounted for by noting that the photoquenching of the electric filed modifies the vacancy structure, and it is the relaxation of the vacancy structure back to its initial state that determines how long the effect persists [34].

Modification of the vacancy structure in the passive film on stainless steel has been detected by Breslin *et al*. [52] by using Mott–Schottky analysis, and the persistence time is found to be in good accord with that estimated from a reasonable value for the vacancy diffusivity [33–35]. If it is assumed that Schmuki and Bohni's 'surface states' are, in fact, oxygen vacancies (which are electronic donors), then the two explanations are equivalent and are within the bounds of the PDM.

At this point it is worth inquiring whether there is any common ground between the stochastic and deterministic views of passivity breakdown. While these two divergent philosophies are not restricted to the present issues, and indeed generally pervade scientific inquiry, there can be no question that the evolution of science is towards determinism. Accordingly, 'science' eventually seeks a deterministic explanation of natural phenomena, because it is only through determinism that a deep understanding of mechanisms can be obtained and reliable predictions can be made. The most obvious point of connection between the stochastic models of Shibata *et al*. [27], Williams and co-workers [45], and Wu *et al*. [46], and the deterministic theory described above, is in the pit generation rate. Thus, using the terminology of Williams *et al*. [45], the rate of generation of stable pits (Λ) is related to the rate of generation of metastable pits (λ) by

$$\Lambda = \lambda \exp(-\mu\tau_c) \tag{17}$$

where μ is the survival probability and τ_c is the critical age of the pit nucleus. The metastable pit generation rate (λ) is given by Equation 16, in PDM parlance. Although, a fully deterministic model for describing the transition from metastable pitting to stable pitting is ultimately desired, it is stressed that the stochastic approach has considerable merit, because it leads to a natural simulation of the fluctuations in the current [46]. However, for this approach to be truly effective, deterministic models must be developed for estimating μ and τ_c.

The issue of 'commonality in mechanism' is of the utmost importance in defining the cause of passivity breakdown. Thus, a multitude of mechanisms have been proposed for passivity breakdown in specific systems, ranging from chloride penetration [53], to electrostrictive rupture [36], to inclusion dissolution [54], but in fact all of the systems for which these mechanisms are proposed display common experimental correlations. For example, they generally display $V_c \propto -\log(a_x)$, with the proportional constant being less than 2.303FT/F. Furthermore, $\log(t_{ind})$ is found to vary inversely with $-\Delta V$. It would be a remarkable quirk of nature if all of these diverse mechanisms gave rise to the same relationships between the dependent (V_c, t_{ind}) and independent (a_x,V, pH) variables. A much more likely explanation is that there exists a *common* mechanism for the initial passivity breakdown event, and it is suggested here that the event is vacancy condensation. Thus, with reference to the stainless steels, where the breakdown

sites have been identified as MnS inclusions, it was previously suggested [1] that the intersection between the barrier oxide layer and the sulfide inclusion represents a region of great lattice mismatch, and hence a region of high cation vacancy diffusivity. Thus, the point of intersection between the barrier layer and the inclusion is (according to the PDM) a preferred site of cation vacancy condensation and therefore of passivity breakdown. Accordingly, it is proposed that the initial breakdown event is that described by the PDM, and that sulfide dissolution and the production of thiosulfate and elemental sulfur, which is observed to decorate the external surfaces [55], occur at a later stage. Breakdown at the point of intersection between the film and the inclusion would clearly lead to the formation of a crevice, which would then acidify as spatially separated anodes and cathodes develop at the breakdown site. The formation of acidic conditions in the crevice would then lead to MnS dissolution, and the HS^- ion produced by this reaction eventually would be oxidized to $S_2O_3^{2-}$ and elemental sulfur as it diffuses into the external environment. This scenario explains the dependence of V_c and t_{ind} on a_x that is observed experimentally, and which does not appear to be explainable in terms of MnS dissolution alone.

Repassivation

The kinetics of repassivation of localized corrosion events has a profound impact on the accumulation of damage. Two, fundamentally different passivation mechanisms may be identified: (i) 'Prompt' repassivation that is responsible for the death of the initial event, and which gives rise to 'metastable pitting', and (ii) 'delayed' passivation that is responsible for the deaths of stable pits at much longer times. Prompt repassivation has been dealt with extensively by Galvele *et al*. [39,56], Burstein and co-workers [57,58], Frankel *et al*. [4,59], and Williams and co-workers [22], and it is attributed to the failure of the nucleus to achieve critical conditions, as expressed by the product of the pit current density and pit radius or inverse radius exceeding a critical value for an individual pit to transition from metastability to stability [60]. The basic idea is that critical conditions, due to the spatial separation of the partial anode (in the crevice) and the partial cathode (on the external surface) must be achieved for the pit to grow to a self-sustaining condition. An important concept in determining the probability of survival of a pit, particularly at an early age, is the continued integrity of the cap. Massive rupture of the cap at a time that is too early in the life of a nucleus would result in dispersal of the aggressive solution that has accumulated within the crevice, and hence would lead to repassivation [30]. On the other hand, lack of communication between the crevice and the external environment may result in the unsustainability of the spatially separated partial anode and partial cathode, again resulting in death of the embryo. Clearly, the probability that a pit nucleus will survive is a sensitive function of the history of the cap, and any model that is proposed to explain prompt repassivation ultimately will have to address the fate of the post-breakdown barrier layer blister.

The story with regard to 'delayed' passivation is quite different. The basic phenomena were observed more than a decade ago by Lenhart, English & Macdonald [61], who investigated the nucleation and growth of pits on nickel in buffered chloride solution by observing the surface *in situ* using optical microscopy. Each pit that nucleated on the surface and grew had associated with it a 'hemisphere of influence' (HOI), centered on the pit mouth. The HOI, which is produced by a high concentration of hydrolyzed metal ions and is clearly visible under optimal conditions of illumination, increased in radius as the pit aged. Two important observations were made: (i) No new, stable pits nucleated under the HOI of an existing pit, and (ii) the overlap (or more accurately the extent of the impingement) of the HOIs from neighboring pits inevitably lead to the death of one of the pits. The first observation can be attributed to the fact that a pit cathodically protects the external surface under the HOI, due to the preponderance of the cathodic partial current on the surface, and indeed this has been predicted theoretically [62]. The second observation reflects the competition between pits for the available resources on the external surface. Thus, if the pits grow independently without interaction of the two HOIs, sufficient resources are available for each pit to grow and each will develop independently. However, when the HOIs of neighboring pits impinge upon one another, the pits compete for the same resources (oxygen reduction) on the external surface, and if insufficient resources are available for both pits to grow, then only the fittest survives in a process that is Darwinian in nature. The author regards the deterministic modeling of this phenomenon as one of the most challenging tasks in corrosion science and electrochemistry.

THE DETERMINISTIC PREDICTION OF DAMAGE

The development of a deterministic theory for passivity breakdown (i.e. a theory whose output is constrained by the relevant natural laws), such as the PDM outlined above, provides an opportunity for predicting localized corrosion damage under conditions that cannot be addressed by empirical methods [1,62–65]. This goal has been achieved to a significant extent by combining the PDM with a deterministic model for pit growth and by assuming a first order kinetic law for delayed repassivation [63]. Typical examples of damage functions (DFs), which are histograms of the event frequency (number per unit area) vs. increment in depth, are shown in Fig. 12 as a function of the observation time. In this particular calculation, which employed parameter values corresponding to passivity breakdown on iron [63], moderate delayed repassivation conditions ($\gamma = 1$/year) were assumed, and the DFs were derived for a given chloride concentration (0.571×10^{-3} M), pH (= 7) and potential ($E_{corr} = -0.334$ V_{SHE}). The conditions chosen are such that all of the pits nucleate within a time interval corresponding to the first depth increment. Thus, the pits shown at depths between 0 and 0.12 cm for $t_{obs} = 0.5$ years are dead (passivated), while those at the largest depth are still active. As the observation time increases, the maximum depth of the damage also increases (to ~ 6.5 mm after 5 years) and the number of active pits is drastically reduced. Note that the DF provides a convenient definition of the 'failure time' as corresponding to that observation time at which the upper extreme exceeds some critical dimension (e.g. the thickness of a pipe wall).

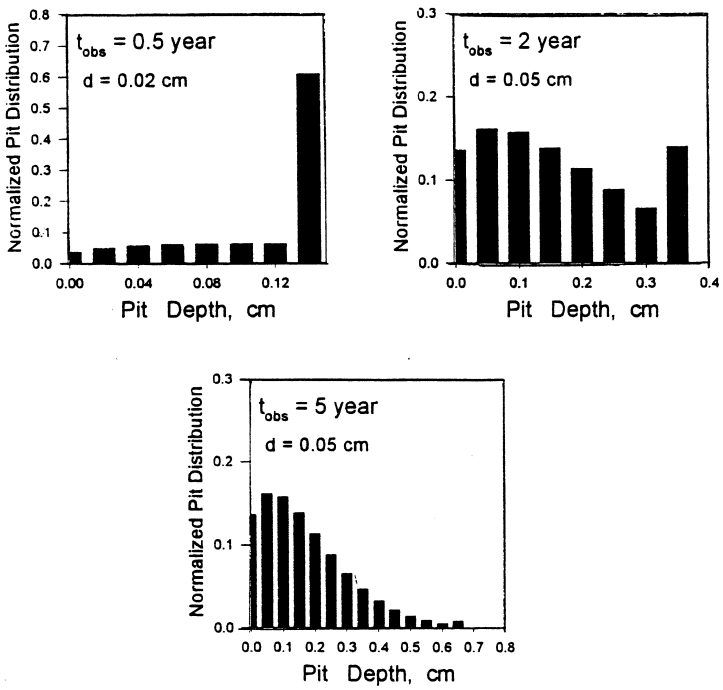

Fig. 12 The influence of observation time on the normalized pit distributions in the pitting of steel in chloride-containing water. $C_{NaCl} = 0.571 \times 10^{-3}$ mol/L, $E_{corr} = -0.334$ V, pH = 7, T = 25 °C, and $\gamma = 1$/year.

The delayed repassivation constant, γ, has a profound effect on the evolution of pitting damage on a metal surface, as shown in Fig. 13. Again, the parameter values were chosen such that all of the (stable) pits nucleate at very short times. This was done in order to illustrate the importance of delayed repassivation, alone, in determining the form and extent of damage. The DFs shown in Fig. 13 for $\gamma = 0$ and for an observation time of 1.0 years consists of the full population of stable pits at a single (maximum) depth, as expected. All of these pits are active and would continue to grow in unison in the absence of repassivation phenomenon. As γ increases, and hence the rate of delayed repassivation becomes greater, passivated ('dead') pits populate smaller depths and the number of active pits at the greatest depth decreases. At the largest value of γ chosen (5/year), the great majority (> 99%) of pits are dead. Now, the

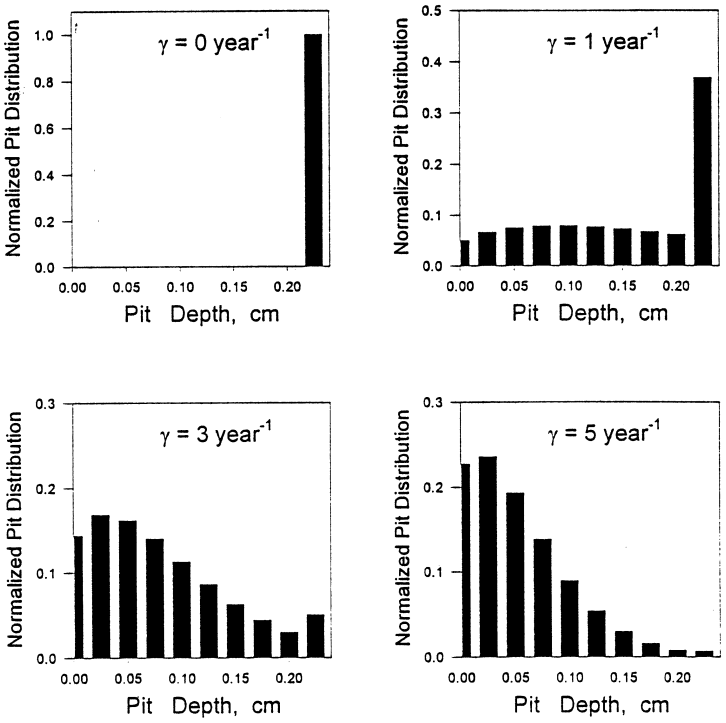

Fig. 13 The influence of the repassivation constant, γ, on the normalized pit distribution in the pitting of steel in chloride contaminated water. $C_{NaCl} = 0.571 \times 10^{-3}$ mol/L, $E_{corr} = -0.334$ V, pH = 7, T = 25 °C, $t_{obs} = 1$ year, and d = 0.025 cm. Parameter values are explained in [63].

ordinate in these particular DFs is a probability (P), so that if the product PxN_0, where N_0 is the surface density of breakdown sites, for a given increment is less than one, no pits would be observed (i.e. only integer numbers of pits can exist). Thus, for the particular case shown in Fig. 13, all pits may be dead if N_0 is sufficiently small. The same arguments apply for specimens of different areas; in that case, AxN_0 where A is the specimen area, may be sufficiently small that $PxAxN_0 < 1$ for one or more of the deepest segments, and hence no pits will be observed at those depths. Thus, the probability of finding a pit of a given depth increases with increasing size of the specimen, which is a well-established experimental observation that is commonly rationalized on the basis of extreme value statistics.

As noted above, the parameter values chosen for the calculations shown in Figs 12 and 13 were such that the entire population of stable pits had nucleated within the first depth increment. This particular case is referred to as 'instantaneous' nucleation and growth. The more general case of progressive nucleation and growth is when new (stable) pits nucleate as existing pits grow and die. Examples of this case, in which parameter values were chosen to ensure continued nucleation beyond the first increment, are shown in Figs 14, 15 and 16, which simulate pitting damage on steel ball bearings in contact with water-contaminated oil [66]. In this case, the DF (Fig. 14) is deconvolved into separate DFs for active pits (Fig. 15) and for passivated (dead) pits (Fig. 16). One can see from Fig. 14 that new, stable pits have nucleated throughout the entire observation period. Furthermore, the populations of both the active pits (Fig. 15) and passivated pits (Fig. 16) change in a complimentary manner, primarily because they are related through the assumed repassivation law. The ability to deconvolve the DF into active and inactive components is proving to be of great theoretical importance in developing new strategies to control localized corrosion, because of the emphasis that is placed on the physico-electrochemistry of pit repassivation and survival.

The methods outlined above have now been used to predict failure times for a number of specific systems, including stainless steel condensing heat exchangers [65], low pressure steam turbines (due to pitting/stress corrosion cracking) [64], and steel ball bearings in contaminated oil [66]. In the first case, the failure of condensing heat exchanges, pitting occurs under a thin condensate film that forms on the

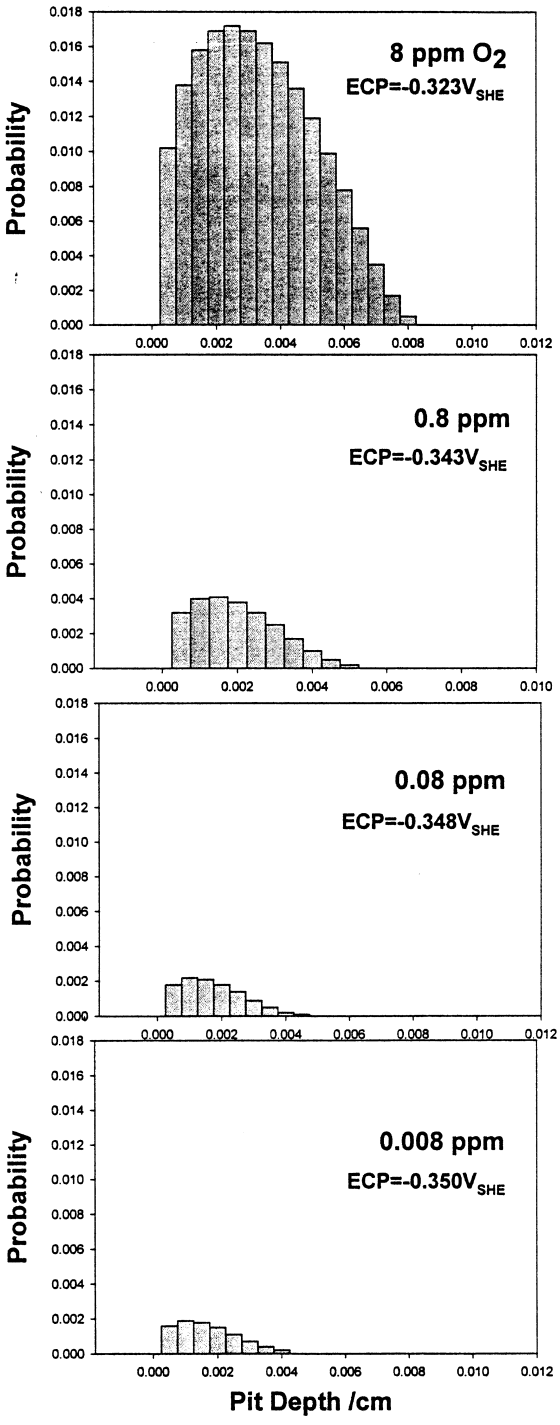

Fig. 14 Calculated pitting damage functions for high-strength steel ball bearings in water-contaminated oil as a function of oxygen concentration. [NaCl] = 10^{-6} M, T = 25 °C, γ = 10/year, t_{obs} = 0.154 years, pH = 5.31, $\bar{V}_c = -0.097V_{SHE}$.

flue side of the stainless steel (Type 304L) heat exchanger [65]. Because of the aggressiveness of this environment, delayed pit repassivation was judged to be unimportant, but the damage was considered to evolve in a progressive nature. The calculated failure times, for a given duty cycle (i.e. sequence of on/off periods for the burner, and hence for cyclical variations in the gas composition), were compared with

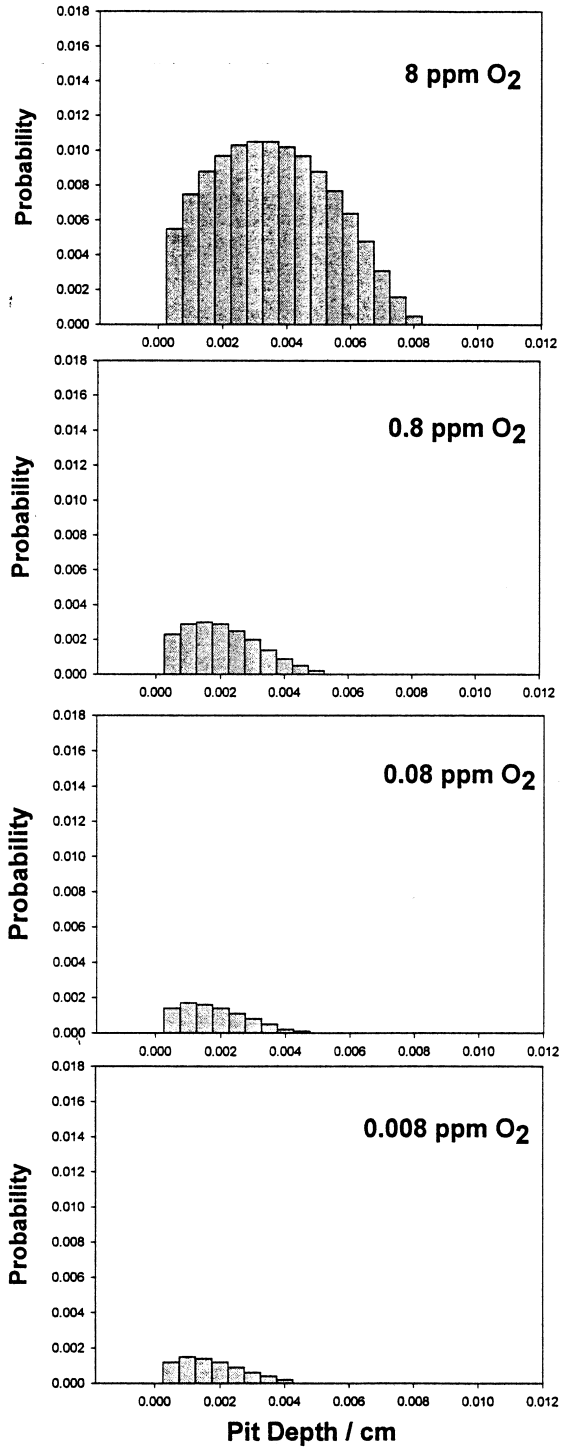

Fig. 15 Calculated damage functions for active pits on high-strength steel ball bearings in water-contaminated oil as a function of oxygen concentration. [NaCl] = 10^{-6} M, T = 25 °C. Other parameters are given in Fig. 14.

those measured in instrumented heat exchangers by the Battelle Columbus Laboratories in a double-blind manner [65]. The results are plotted in Fig. 17 as a function of the chloride concentration. Although experimental failure times were available for only the two highest chloride concentrations, the calculated failure times were found to be in good agreement with the measured values.

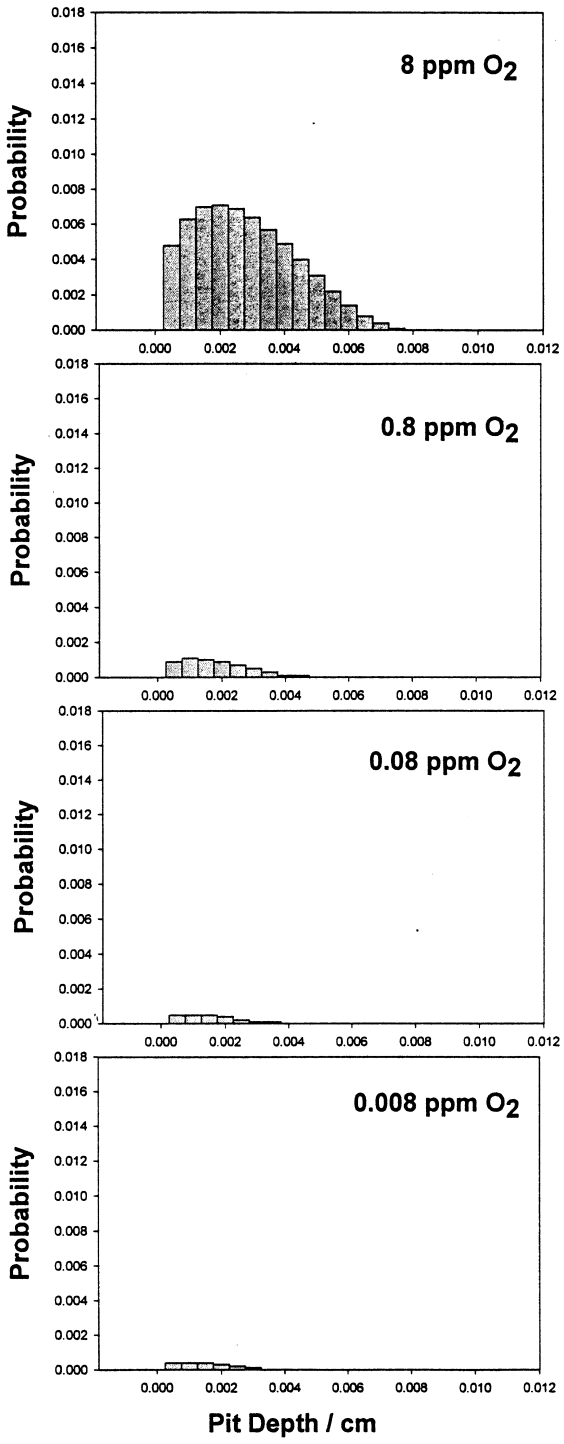

Fig. 16 Calculated damage functions for passivated pits on steel ball bearings in water-contaminated oil as a function of oxygen concentration. [NaCl] = 10^{-6} M, T = 25 °C. Other parameters are given in Fig. 14.

In the case of the low-pressure steam turbines [64], pits were postulated to act as nucleation sites for cracks, with failure occurring via mechanical overload after a period of slow crack growth, the rate of which was calculated deterministically. Again, the calculated failure times were found to be in good agreement with laboratory and field data [64].

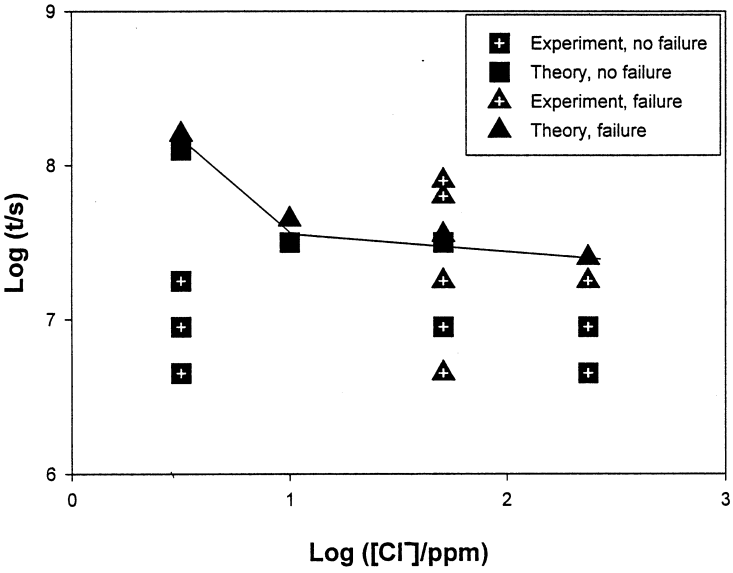

Fig. 17 Comparison of measured and calculated service lives of Type 304L condensing heat exchanger tubes as a function of chloride concentration. The duty cycle and parameter values are given in [65].

The deterministic prediction of damage is in its infancy, with the basic concepts only now being formulated. However, the initial work in this area, as summarized above, has demonstrated the practical feasibility of predicting damage in a deterministic manner, and it is expected that the techniques outlined in this paper will evolve into powerful tools for scheduling maintenance, assessing risk, and specifying design parameters in complex industrial systems.

ACKNOWLEDGEMENTS

The author gratefully acknowledges the support provided by the organizers of the 7th International Chemistry Conference of Africa, Durban, South Africa. The support of SRI International and The Pennsylvania State University in preparing this paper is also gratefully acknowledged.

REFERENCES

1 D. D. Macdonald. *J. Electrochem. Soc.* **139**, 3434 (1992).

2 N. Sato. *Passivity of Metals* (R. P. Frankenthal, J. Kruger, eds), p. 29. The Electrochemical Soc., Princeton, NJ (1978).

3 H. H. Uhlig. *Passivity of Metals* (R. P. Frankenthal, J. Kruger, eds), p. 1. The Electrochemical Soc., Princeton, NJ (1978).

4 G. S. Frankel. *J. Electrochem. Soc.* **145**, 2186 (1998).

5 R. P. Franenthal, J. Kruger, eds. *Passivity of Metals.* The Electrochemical Society, Princeton, NJ (1978).

6 M. Fromont, ed. *Passivity of Metals and Semiconductors.* Elsevier, Amsterdam (1983).

7 L. Young. *Anodic Oxide Films.* Academic Press, New York (1961).

8 P. M. Natishan, *et al.*, eds. *Passivity and its Breakdown*, Proc. Vol. PV97-26, the Electrochemical Society, Princeton, NJ (1998).

9 S. Glasstone. *An Introduction to Electrochemistry*, p. 491. Van Nostrand, New York, NY (1942).

10 M. Pourbaix. *Atlas of Electrochemical Equlibria.* NACE-International, Houston, TX (1973).

11 D. D. Mcdonald, S. R. Biaggio, H. Song. *J. Electrochem. Soc.* **139**, 170 (1992).

12 K. Ismail, D. D. Macdonald, E. Sikora. *J. Electrochem. Soc.* **145**, 3141 (1998).

13 E. J. W. Vervey. *Physica* **2**, 1059 (1935).

14 N. Cabrera, N. F. Mott. *Report Progr. Phys.* **12**, 163 (1948).

15 K. J. Vetter, F. Gorn. *Electrochim. Acta* **18**, 321 (1973).

16 N. Sato, M. Cohen. *J. Electrochem. Soc.* **111**, 512 (1964).

17 R. Kirchheim. *Electrochim. Acta* **32**, 1619 (1987).

18 E. Sikora, D. D. Macdonald, J. Sikora. *Proc. 7th Int. Symp. Oxide Films, Mets. Alloys* (K. R. Herbert, G. E. Thompson, eds), PEC, **94–25**, 139 (1994).

19 C.-Y. Chao, L. F. Lin, D. D. Macdonald. *J. Electrochem. Soc.* **128**, 1187 (1981).

20 L. Zhang, D. D. Macdonald, E. Sikora, J. Sikora. *J. Electrochem. Soc.* **145**, 898 (1998).

21 O. Pensado-Rodriquez, J. Flores, M. Urquidi-Macdonald, D. D. Macdonald. The electrochemistry of lithium in alkaline aqueous solutions, part II. Point defect model. *J. Electrochem. Soc.* **146**, 1326 (1999).

22 D. E. Williams, J. Stewart, P. H. Balkwill. *Corros. Sci.* **36**, 1213 (1994).

23 Z. Szklarska-Smialowska. *Pitting Corrosion of Metals.* NACE, Houston, TX (1986).

24 P. C. Pistorius, G. T. Burstein. *Phil. Trans. Roy. Soc., A* **341**, 531 (1992).

25 G. S. Frankel, L. Stockert, F. Hunkeler, H. Bohni. *Corrosion* **43**, 429 (1987).

26 S. Lenhart, C. English, D. D. Macdonald. unpublished data (1988).

27 T. Shibata, T. Takeyama. *Corrosion* **33**, 243 (1977).

28 L.-F. Lin, C.-Y. Chao, D. D. Macdonald. *J. Electrochem. Soc.* **128**, 1194 (1981).

29 D. Ellerbrock, D. D. Macdonald. *Mat. Sci. Forum* **185–8**, 927 (1995).

30 N. J. Laycock, S. P. White, J. S. Noh, P. T. Wilson, R. C. Newman. *J. Electrochem. Soc.* **45**, 1101 (1998).

31 S. Lenhart, M. Urquidi-Macdonald, D. D. Macdonald. *Electrochim. Acta* **32**, 1739 (1987).

32 P. Schmuki, H. Bohni. *Electrochim. Acta* **40**, 775 (1995).

33 D. D. Macdonald, E. Sikora, M. W. Balmas, R. C. Alkire. *Corros. Sci.* **38**, 137 (1997).

34 C. B. Breslin, D. D. Macdonald, E. Sikora, J. Sikora. *Electrochim. Acta* **42** (127 (1997); **42**), 137 (1997).

35 D. Heaney, D. D. Macdonald. *J. Electrochem. Soc.* (1998), in press.

36 T. Okada. *J. Electrochem. Soc.* **131**, 241 (1984).

37 K.-S. Lei, D. D. Macdonald, B. G. Pound, B. E. Wilde. *J. Electrochem. Soc.* **135**, 1625 (1988).

38 I. Milosev, M. Metokos-Hukovic, M. Drogowska, H. Menard, L. Brossard. *J. Electrochem. Soc.* **139**, 2409 (1992).

39 K. Sugimoto, S. Matsuda, Y. Ogiwara, K. Kitamura. *J. Electrochem. Soc.* **132**, 1791 (1985).

40 J. R. Galvele. *Corrosion—Aqueous Processes and Passive Films*, Vol. 23 of *Treatise on Materials Science and Technology* (J. R. Scully, ed.), p. 1. Academic Press, New York (1983).

41 C. B. Bargeron, R. B. Givens. *J. Electrochem. Soc.* **124**, 1845 (1977).

42 C. B. Bargeron, R. B. Givens. *Corrosion* **36**, 618 (1980).

43 T. Haruna, D. D. Macdonald. *J. Electrochem. Soc.* **144**, 1574 (1997).

44 N. Casillas, S. Charlebois, W. H. Smyol, H. S. White. *J. Electrochem. Soc.* **140**, L142 (1993); N. Casillas, S. Charlebois, W. H. Smyol, H. S. White. *J. Electrochem. Soc.* **141**, 636 (1994).

45 D. E. Williams, C. Westcott, M. Fleischmann. *J. Electrochem. Soc.* **132**, 1796 (1985).

46 B. Wu, J. R. Scully, J. L. Hudson, A. S. Mikailov. *J. Electrochem. Soc.* **144** (1614 (1997); **144**), 1620 (1997).

47 D. D. Macdonald, M. Urquidi-Macdonald. *Electrochim. Acta* **31**, 1070 (1986).

48 M. Urquidi-Macdonald, D. D. Macdonald. *J. Electrochem. Soc.* **134**, 41 (1987).

49 D. D. Macdonald, M. Urquidi. *J. Electrochem. Soc.* **132**, 555 (1989).

50 H. Brookes, M. Vasquez, D. D. Macdonald. *Corrosion* **55**, 343 (1999).

51 S. Fugimoto, T. Yamada, T. Shibata. *J. Electrochem. Soc.* **145**, L79 (1998).

52 C. B. Breslin, E. Sikora, D. D. Macdonald. unpublished data (1998).

53 T. P. Hoar. *Corros. Sci.* **5**, 279 (1965).

54 J. Stewart, D. E. Williams. *Corros. Sci.* **33**, 457 (1992).

55 R. Ke, R. Alkire. *J. Electrochem. Soc.* **139**, 1573 (1992).

56 J. R. Galvele. *Corros. Sci.* **21**, 55 (1981); J. R. Galvele. *J. Electrochem. Soc.* **122**, 465 (1976).

57 P. C. Pistorius, G. T. Burnstein. *Corros. Sci.* **33**, 1885 (1992).

58 P. C. Pistorius, G. T. Burnstein. *Phil. Trans. R. Soc. Lond. A* **341**, 531 (1992).

59 G. S. Frankel. L. Stockert, F. Hunkeler, H. Bohni. *Corrosion* **43**, 429 (1987).

60 H. Ezuber, R. C. Newman. *Critical Factors in Localized Corrosion* (G. S. Frankel, R. C. Newman, eds), PV92-9, p. 12. Electrochemical Society, Princeton, New Jersey (1992).

61 D. D. Macdonald, C. English, S. J. Lenhart. *Report to DOE/BES.* SRI International, Menlo Park, CA (1985).

62 C. Liu, D. D. Macdonald. Modeling the failures of low pressure steam turbine disks. In *Proc. 5th International Conference on Nuclear Energy*, ICONES, 25–29 May 1997, Nice, France/ASME, New York.

63 G. Englehardt, D. D. Macdonald. *Corrosion* **54**, 469 (1998).

64 C. Liu, D. D. Macdonald. *J. Press. Vessel Techn* **119**, 393 (1997).

65 D. D. Macdonald, C. Liu, M. Urquidi-Macdonald, G. Stickford, B. Hindin, A. K. Agrawal. *Corrosion* **50**, 761 (1994).

66 G. Englehardt, D. D. Macdonald (1998), to be published.